Translucency and negative temperature-dependence for the slip length of water on graphene

Supplementary Information

Han Li[1,2], Zhi Xu[1,2], Chen Ma[2,3], Ming Ma[1,2]*

[1]Department of Mechanical Engineering, State Key Laboratory of Tribology in Advanced Equipment (SKLT), Tsinghua University, Beijing 100084, China

[2]Center for Nano and Micro Mechanics, Tsinghua University, Beijing 100084, China

[3]Department of Engineering Mechanics, Tsinghua University, Beijing 100084, China

In this supplementary information, we provide additional details on certain aspects of the study reported in the manuscript. The following issues are discussed:

1. Colloidal probe atomic force microscope
2. Experimental section
3. Analysis of surface roughness
4. Error factors analysis
5. Material characterization
6. Theoretical analysis details
7. Velocity-independent slip length
8. Comparison with literature
9. Statistical analysis for temperature dependence results
10. Gauss distribution of slip length results
11. Discussion about the electronic effect and quantum friction

1. Colloidal probe atomic force microscope

1.1 Measurement method

There are several methods to measure the slip length, in this paper, we apply the colloidal probe atomic force microscope (CP-AFM) method, which is one of the most common-used. the main advantages of CP-AFM are the high resolution and generality. The resolution of slip length measured by CP-AFM can reach ~0.7 nm according to our estimation, while other methods such as micro/nano-channel, quartz crystal microbalance, particle image velocimeter can’t reach this accuracy. Besides, surface force apparatus can also

get a slip length with nanometer accuracy, but its generality is not as good as AFM[1].

To improve the accuracy of our results, we do force curves in three different piezo-velocities (75, 100, 150 μm/s) on each measured location, and the number of force curves are more than 50 at each preset velocity. The final results are the averages and distributions of all these thousands of force curves.

The CP-AFM method is applied as Figure 1a in the main text. The colloidal probe consists a tipless cantilever (CSC38, Mikromasch Instrument) and a glued microsphere tip (borosilicate glass, 9020, Duke Scientific). The microsphere is used to increase the force signal acting on the probe. In AFM, a laser beam is focused onto the end of the cantilever, and the reflected signal is detected by a photo detector, constructing an optical lever system. During the measurement, the probe and sample are immersed into degassed deionized water, a piezoelectric ceramic drives the sample stage at a preset speed to the probe which is held fixed. Because of the hydrodynamic force on the sphere, the cantilever bends, meanwhile the deflection of cantilever is enlarged and recorded as voltage signal by the optical lever system. When the voltage detected reaching a certain threshold, which named "trigger point" in AFM software, the piezo ceramic controls the sample stage to retract. The relationship between force signal detected by photo detector and the piezo-displacement in the whole process is recorded, named "force distance curve".

The raw force distance curves give the relationship between voltage detected by photo detector and the piezo-displacement. However, to calculate the slip length, what we need actually is the relationship between the hydrodynamic force and the tip-sample separation. As a result, the raw force curves need to be converted. The conversion process is a standard method which can refer to the exhaustive review proposed by H. J. Butt et al[2].

The theoretical hydrodynamic force between the spherical tip and the flat sample is deduced by O. I. Vinogrodova et al[3]. They substituted the slip boundary condition into Navier-Stokes Equation and calculated the hydrodynamic drainage force F_{h} of a sphere approaching to a plane:

$$F_{\mathrm{h}} = \frac{6\pi R^2 \mu v}{h} f^* \qquad (S1.1)$$

In formula (S1.1), R is the radius of microsphere, μ is the viscosity of liquid, v is the velocity of the sphere surface, $v = \dot{h}$, f^* is a correction factor related with the slip length. If the two surfaces have the same slip length l_{s}, then:

$$f^* = \frac{h}{3l_{\mathrm{s}}}\left[\left(1 + \frac{h}{3l_{\mathrm{s}}}\right)\ln\left(1 + \frac{6l_{\mathrm{s}}}{h}\right) - 1\right] \qquad (S1.2)$$

The formula (S1.2) is available for the case of small Reynolds number, rigid surfaces, Newton fluid, and the radius $R \gg h$. It is the basic principle of AFM slip length measurement, however, the parameter f^* is

complicated and difficult to fit. To overcome this problem, the formulas (S1.1) and (S1.2) is further approximated by D. F. Honig, W. Ducker, and C. Cottin-Bizonne et al[4, 5]. In the case that $h \gg l_s$, it can be approximated as:

$$\frac{v}{F_h} = \frac{h + l_s^{total}}{6\pi R^2 \mu} \qquad (S1.3)$$

l_s^{total} is the total slip length of the tip and sample, $l_s^{total} = l_s + l_s^{tip}$ with l_s as the slip length of the flat measured surface. Compared with formulas (S1.1) and (S1.2), formula (S1.3) is more easily to be fitted. For most measurements including our experiments, hydrophilic spheres such as silica and glass are chosen as the tips, thus, $l_s^{tip} = 0$, $l_s^{total} = l_s$. Figure 1e in the main text gives the converted $v/F_h - h$ curve. The red line is the data of approaching process while the blue is the retraction. Both of the lines are close to each other, according to W. Ducker et al[5]. it means the correctness of our data analyze. The slope of Figure 1e is the combination of R, μ, and the opposite of the intercept of the extended linear region on the horizontal axis is the apparent slip length. In our experiments, we first measure the force curves of mica, because mica is regarded as an extremely hydrophilic materials whose slip length is zero, the slip length measured on mica is regarded as the possible constant systematic error lead by the probe. Then we change the sample to other materials to measure the other slip length using the same probe. The deviation between the two slip length values is the true apparent slip length of the latter surface.

For l_s on graphene (brown area in Figure 1a in the main text) with different supporting substrates, the morphology of the surface was recorded at first. According to T. Lee, E. Charrault and C. Neto et al,[1] the radius of the contact area that mainly affects the hydrodynamic force is about $\sqrt{2Rh}$. In our measurements, h is smaller than 4 μm, and R is ~10 μm, lead to $\sqrt{2Rh} \cong 9$ μm. The area of our graphene samples is much larger than 20×20 μm^2, which is large enough to ensure that the influence of bare substrate which is not covered by graphene can be neglected. Besides, the values of root mean square (RMS) roughness for graphene on substrates are measured to be about 0.6~0.8 nm, close to that of the substrates. Such small roughness could eliminate the influence of surface morphology on the measurement of l_s. [1]

Besides, there are many other factors that may lead to error, such as the surface roughness, surface force, thermal noise, inverse optical lever sensitivity, zero points of separation and force, etc. These factors are analyzed in the following section 4. We measured the sample and tip roughness before each hydrodynamic force experiment, the tip roughness is calibrated by the standard sample TGT1 (NT-MDT Instrument).

To improve the accuracy of our results, we do force curves in three different piezo-velocities (75, 100, 150

μm/s) on each measured location, and the number of force curves are more than 50 at each speed. The final results are the averages and distributions of all these thousands of force curves.

1.2 Discussions on the Vinogradova assumptions.

In the above, we have introduced the theory of O. I. Vinogradova et al, $F_{\mathrm{h}} = \frac{6\pi R^2 \eta v}{h} f^*$, where F_h is the hydrodynamic force, R is the tip radius, η is the liquid viscosity, v is the relative velocity between spherical tip and to-be-measured plane surface, h is the separation between the sphere and plane, $f^* = \frac{h}{3l_{\mathrm{s}}}\left[\left(1+\frac{h}{3l_{\mathrm{s}}}\right)\ln\left(1+\frac{6l_{\mathrm{s}}}{h}\right)-1\right]$. There are four assumptions for Vinogradova's theory, which are 1. The solid surfaces are rigid and smooth, the deformation and roughness are neglected. 2. The liquid is Newtonian, isotropic and homogeneous. 3. The Reynolds number is small, and the inertia force can be neglected. 4. $h \ll R$. For our measurement, all of the four assumptions are valid. Here are the detailed discussions.

Discussion for assumption 1, the solid surfaces are rigid and smooth, the deformation and roughness are neglected. The RMS roughness of spherical tip is 1.2 nm, and that of graphene is 0.6~0.8 nm. These values are much smaller than the slip length measured (a few nanometers), and their effects on the slip length measurement are negligible (see section 1.2.2 below regarding the roughness for more details). As the maximum hydrodynamic force acting on the tip in our experiments is about 10 nN (see the force curves in Figure S4c in SI), according to the Hertz theory, the maximum deformation of surfaces is $\delta = \left(\frac{9W^2}{16E'^2R}\right)^{1/3}$, E' is the Young's Modulus, being 170 ~ 190 GPa for silica, and finally the deformation $\delta \cong 5\times10^{-12}$ m $= 0.005$ nm. Such small deformation can be neglected.

Discussion for assumption 2, the liquid is Newtonian, isotropic and homogeneous. The separation region used for slip length calculation is (25, 250) nm in our experiments, where water appears bulk properties. The bulk water is obviously Newtonian, isotropic and homogeneous. The existing slip length measurements for water also regarded water as a Newtonian, isotropic and homogeneous liquid[1, 5-8].

Discussion for assumption 3, the Reynolds number is small, and the inertia force can be neglected. In our experiments, the velocity for liquid v is less than 100 μm/s, and maximum separation h for slip length calculation is 250 nm, the viscosity of water η is 1 mPa·s. Thus, the corresponding $Re = \frac{\rho v h}{\eta} \cong 2.5\times10^{-5}$, which is small and the inertia force can be neglected indeed.

Discussion for assumption 4, $h \ll R$. For slip length calculation in our experiments, $h < 250$ nm, $R = 10^4$ nm, thus, $h/R = 0.025 \ll 1$.

From the above discussions, we can conclude that our experiments satisfy the assumptions by Vinogradova.

Further, the formula we actually used is an approximation of Vinogradova's formula[3, 4]. That is $\frac{v}{F_{\mathrm{h}}} = \frac{h+l_{\mathrm{s}}^{\mathrm{total}}}{6\pi R^2 \mu}$, $l_{\mathrm{s}}^{\mathrm{total}}$ is the total slip length of the tip and sample, $l_{\mathrm{s}}^{\mathrm{total}} = l_{\mathrm{s}} + l_{\mathrm{s}}^{\mathrm{tip}}$ with l_{s} as the slip length of the flat measured surface. The main purpose for such approximation is to simplify the data analysis and reduce error. The condition for such approximation is $h \gg l_s$. In our experiments, l_s~4 nm for graphene and graphite, and $h = 250$ nm, thus such approximation holds. According to the discussion by C. Cottin-Bizonne et al.,[4] if $h/l_s = 10$, the error for the linear fitting for slip length is < 0.7%. They also measured slip length of water on OTS and got a slip length 13~19 nm with maximum separation h as 220 nm for water (Figure 6, 7, 8 in Ref [4]), which is quite close to our measurements and results (13.4±3 nm).

In summary, the basic assumptions of the used formulas are valid for our measurements.

2. Experimental section

The commercial AFM we operated is Cypher ES (Asylum Research, Oxford Instruments). Before the slip length measurement, the sample stage and the tip holder are cleaned by ethanol and DI water streams, and dried by nitrogen gas flow for 10 minutes. The built-in temperature-controlling system in Cypher ES allows us to perform experiments under different temperature. The temperature is controlled by a hot-and-cooling plate mounted on the sample stage, and a temperature detector is also mounted in the cavity. When the temperature changes, the deflection signal will significantly vary with the variation of temperature and finally be stable, which is also called thermal drift in the AFM research. All our experiments are performed after the deflection being stable and the thermal drift being excluded. The analysis in section 4 also mentions the thermal drift.

The colloidal probe in our experiments is made up of a borosilicate glass sphere (Duke Scientific) and a soft rectangular tipless cantilever (CSC38, Mikromash). The sphere is ultraviolet curably glued (ergo 8500) onto the end of the cantilever. Before experiments, probes are cleaned by an oxygen plasma cleaner and measure the morphology of the colloidal probes using a TGT1 standard sample (NT-MDT Instrument) to make sure they are clean and smooth. Contaminated probe may get a strong adhesion in experiments and introduce large error. The RMS roughness of the spherical tip is ~1.2 nm typically. The colloidal probe characterization is listed in section 5.

The graphite sample is highly oriented pyrolytic graphite (HOPG, grade ZYB, GRBS), and the mica is muscovite, purchased from Tedpella. Both HOPG and mica are freshly cleaved before experiments. For the preparation of the substrates with different wettability, the silica wafers are divided into 2 groups, used for the

preparations of graphene on SiO_2 and on OTS, respectively. The first are ultrasonic cleaned in acetone, ethanol and DI water for 10 minutes respectively, and then cleaned by oxygen plasma. The second are cleaned in piranha solution (98% H_2SO_4 + 30% H_2O_2, volume ratio 7:3) at 120 ℃ for at least 60 minutes, then cleaned in DI water and dried. After the second group cleaned, they are put into the OTS solution (OTS + hexadecane, volume ratio 1:250). Graphene is exfoliated onto the silica and OTS using M3 scotch, and the thickness of the samples is characterized by optical microscope, Raman spectra and AFM respectively. Figure 1b and 1c in the main text gives the AFM and Raman characterization of a 2-layer graphene sample in our experiments, all of the samples are smooth so the influence of roughness on slip length is small (section 4: Error factors analysis). More details about the graphene are listed in section 5: Materials characterization.

3. Analysis of surface roughness

In the main text, we report the slip length translucency phenomenon, we notice that a possible critical factor for our measurements is the surface roughness. With the thickness increasing, the morphology of supported graphene may evolute from the morphology of the substrate to the graphite. In view of the close relationship between slip length and surface roughness[1, 9, 10], a natural conjecture about the slip length translucency is that the variation of slip length may be due to the change of solid surface roughness. To validate this conjecture, we reinspect the morphology of FLG samples and perform an analysis based on the two-dimensional discrete Fourier transform (FT).

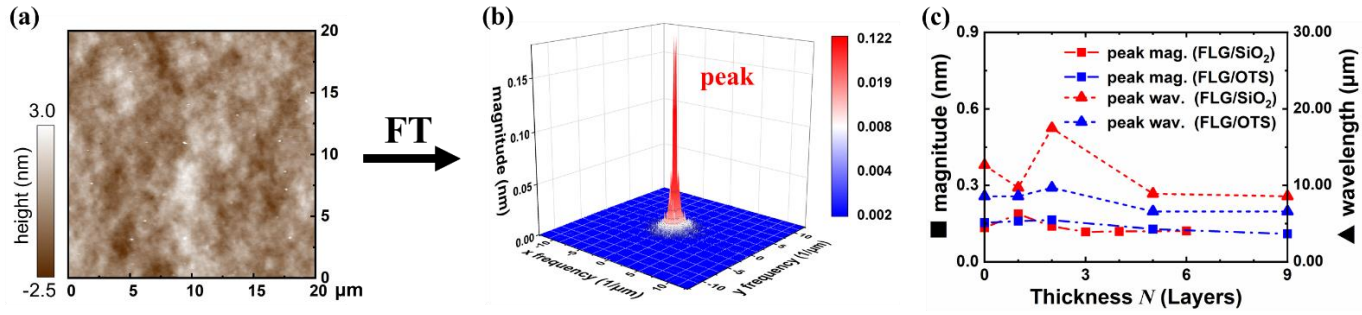

Figure S1. Two-dimensional Fourier transform (FT) analysis of the graphene morphology. (a) Raw image of the SLG/SiO_2 morphology. (b) The corresponding FT image in the frequency domain of Figure S1a, obviously, the low frequency (or large wavelength) component is dominating in the morphology. (c) The corresponding magnitudes and wavelengths of the dominating components (peaks) in FT images for graphene with different thickness *N* and supporting substrates, the wavelengths are calculated from the inverse of the x, y frequency for the peak in Figure S1b.

The two-dimensional FT means that any given surface can be always uniquely equivalent to the sum of a series of sinusoidal surfaces with different magnitude and frequency (or wavelength). In other words, the Fourier transform images reflects the frequency domain properties of the measured morphology. As Figure S1 a, b shows, the FT image is calculated from the raw morphology of graphene. Obviously, the peak is close to the origin point (0, 0) in the frequency domain, which indicates that the morphologies of all images are similarly dominated by the components with low frequency. We calculate the FT image for all FLG samples, and the corresponding magnitudes and wavelengths of the dominating peaks are shown in Figure S1c, indicating the weight of the dominating low frequency components. The FT images are shown in Figure S2. Details about the raw morphology of FLG are given in Section 5. As Figure S1c shows, poor relation between magnitude and the thickness is observed, and the wavelength of low frequency components is about 7~10 μm. As a result, all of the above discussion indicates that the FLG samples applied here possess morphology with similar Fourier components, quantitively indicating the similarity of the morphology. Accompanied with the discussion about the roughness in the main text, we can conclude that the roughness and the morphology are hardly correlated with the slip length. As a result, the slip length translucency is unlikely due to the change of roughness and morphology. In addition, according to the existing consensus[1, 9, 10], the slip length is negatively related to the solid surface roughness in Wenzel regimes because the corrugation of solid surface increases the energy barrier which leads to larger solid-liquid friction. Based on this law, the slip length on FLG/OTS should increases with the thickness because the increasing thickness flatten the surface, however, the results are exactly the opposite, indicating that the roughness is not the reason of the slip length variation. Finally, for FLG with thickness larger than 3, the RMS roughness of FLG/SiO_2 and FLG/OTS is quite different, however the measured slip length here is quite close, also indicating that the roughness is not the reason of the slip length translucency.

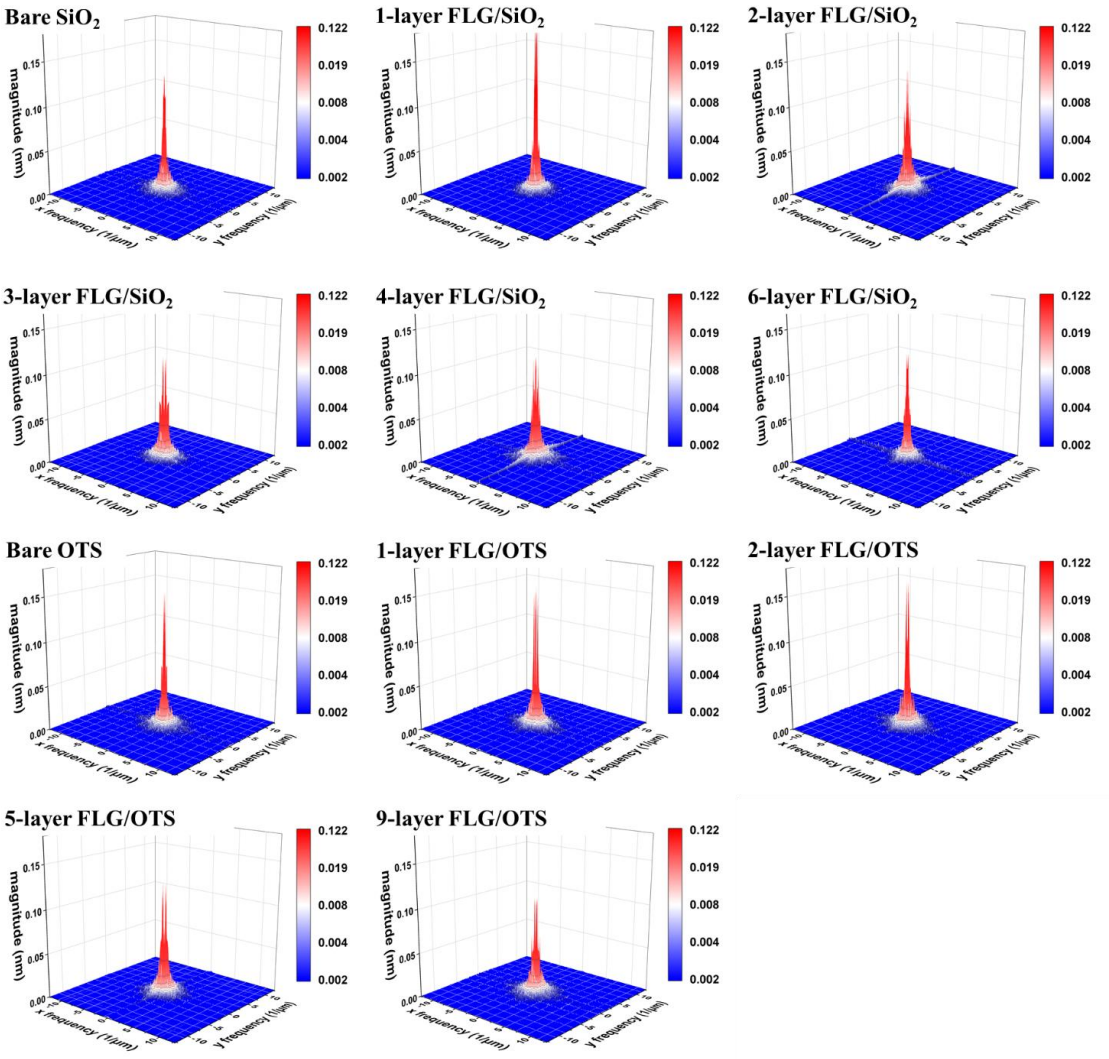

Figure S2. FT images of all graphene samples and substrates.

Except for the direct effect on slip length, the definition accuracy of separation h may also be affected by the surface roughness of both spherical tip and FLG samples[1], called "shifted boundary" in the literature[1]. It indicates that for rough surface, if the characteristic wavelength λ of the surface morphology is smaller than $\sqrt{2Rh}$, the liquid confined between the peaks and valleys on the surface will lead to error in the hydrodynamic force measurement. To counteract such error, the separation needs to be shifted as Figure S3 shows, $h = h_{app} + \delta h$, where h_{app} is the apparent separation calibrated from the AFM force curve, δh is the shifted value, which usually close to the PV or RMS roughness of the solid surface. As mentioned in section 1, the hydrodynamic force $F_{\mathrm{h}} = \frac{6\pi R^2 \mu v}{h} f^*$ can be simplified to $\frac{v}{F_{\mathrm{h}}} = \frac{h + l_{\mathrm{s}}^{\mathrm{total}}}{6\pi R^2 \mu}$ on the basis of $h \gg l_{\mathrm{s}}$. Together with the "shifted boundary", it can be further expressed as $\frac{v}{F_{\mathrm{h}}} = \frac{h_{app} + \delta h + l_{\mathrm{s}}^{\mathrm{tip}} + l_{\mathrm{s}}}{6\pi R^2 \mu} = \frac{h_{app} + \delta h + l_{\mathrm{s}}}{6\pi R^2 \mu}$, with $l_{\mathrm{s}}^{\mathrm{tip}} = 0$ for our used borosilicate glass spheres. As a result, the inaccuracy due to the surface roughness is linear to the slip length.

For the roughness of spherical tip, before each measurement on FLG, we first measure the apparent slip length on mica whose true slip length is zero, the apparent slip length on mica can be regarded as the δh induced by the tip. Then we subtract the slip length on mica from the slip length on FLG to exclude effect of the tip. Similar subtraction is also mentioned in the literature.[11]

For the roughness of FLG, in our experiments, $R = 10$ μm and $h = 200$ nm, thus $\sqrt{2Rh} = 2$ μm, and according to Figure S1c, the wavelength λ of the dominating low frequency components for most samples is about 7~10 μm, much larger than the $\sqrt{2Rh}$. This conclusion also coincides with the raw morphology images in Figure 3 a~c in the main text: although the peak-to-valley roughness is about 6 nm, the lateral distances between peaks and valleys are larger than 5 μm, 1000 times larger than PV roughness, which is quite large by comparison. As a result, as Figure S3b shows, the shifted boundary is not applicable for FLG samples in our experiment, and the measured slip length doesn't need to be shifted.

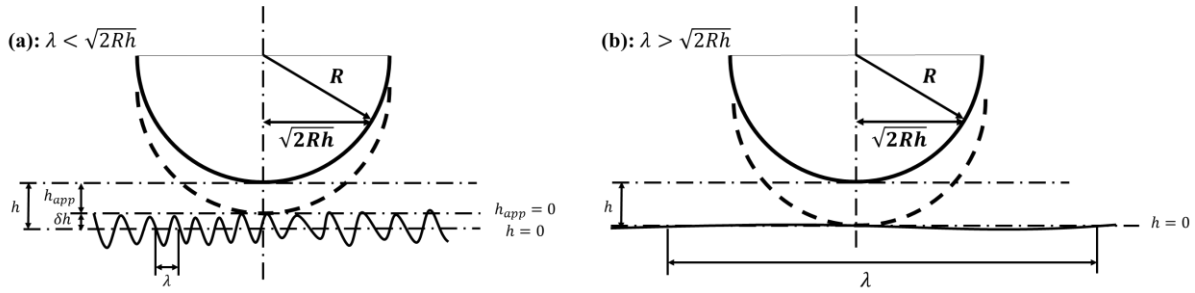

Figure S3. Schematic of shifted boundary. (a) For the roughness with characteristic wavelength $\lambda < \sqrt{2Rh}$, water will be confined between the peaks and valleys of the surface morphology and lead to the deviation of hydrodynamic force. To counteract this effect, the separation h needs to be shifted. (b) For the roughness with characteristic wavelength $\lambda > \sqrt{2Rh}$, no water is confined, the effect of surface morphology is neglectable, h does not need to be shifted. [1]

4. Error factors analysis

Except for the above discussed roughness, there are some other factors that may influence the uncertainty of force curve analysis, former researches in literature have discussed them in detail. To illustrate the accuracy of our measurement, here we list these possible error factors.

Systematic errors:

1) Thermal drift: The Thermal drift is a remarkable error resource of AFM measurement in liquid. In our experiments, the environmental temperature in the AFM cavity is kept at 25°C for more than 20 minutes before force curve measurements to reduce the thermal drift. Besides, the force signal at large separation is nearly

constant and symmetric during the whole approaching and retraction process, as Figure S4 (a) and (b) shows, providing the evidence that the non-existence of thermal drift.

2) Virtual deflection: For head-scanning AFM, the inertia effect of cantilever may lead to a linear drift of deflection at large separation h, which will introduce a large systematic error. But the Cypher ES AFM is stage-scanning, where there is no virtual deflection. In Figure S4 (a) and (b), there is no obvious linear drift in large separation h, giving evidence for the non-existence of virtual deflection.

3) Liquid viscosity and cantilever stiffness: The viscosity of confined water between tip and sample is hard to be measured in situ, however, the accuracy of viscosity directly affects the accuracy of slip length. In our measurement, the spring constant is calibrated by the hydrodynamic method proposed by V. S. J Craig and C. Neto,[12] the advantage is that this method can make the errors of viscosity and cantilever stiffness counteract.

Random errors:

4) Thermal noise: The thermal noise is a key parameter that affect the force resolution of AFM. From Figure S4 (b) we can see that the peak-to-valley thermal noise in our experiment is ~0.04 nN, with corresponding root-mean-square ~0.01 nN, similar to other AFM experiments in literature.

5) Zero Force point: The accuracy of zero force mainly depends on the thermal noise, according to the analysis of thermal noise, in our experiments the corresponding root-mean-square error of zero force point ΔF_h is about $\pm$0.01nN.

6) Roughness of substrate and microsphere: The error introduced by roughness is embodied in the error of contact point[1], which is analyzed in the next.

7) Contact point (zero separation): In AFM, the separation is calculated indirectly, the accuracy of separation mainly depends on the accuracy of contact point and inverse optical lever sensitivity, the typical contact region of force curve is given in Figure S4 (c) and (d), the typical peak-to-valley error of zero separation is smaller than 1nm, with corresponding root-mean-square error <0.2 nm, because of the smooth morphology of graphene.

8) Inverse Optical Lever Sensitivity: The $invOLS$ is least squared fitted according to the linear region of force curve. In our experiments, the $invOLS$ resolution is about 0.5~2 nm/V, with a relative error is about 0.5%~2%. Figure S4 e, f gives the distribution of inverse optical lever sensitivity for 70 force curves measured in the same location on SLG/SiO_2.

Error transfer:

According to $\frac{v}{F_\mathrm{h}} = \frac{h+l_\mathrm{s}}{6\pi R^2 \mu}$, we can get $l_\mathrm{s} = 6\pi R^2 \mu v / F_\mathrm{h} - h$. The main error factors in this formula are

hydrodynamic force F_h and separation h, with standard deviations $\Delta F_h \sim 0.01$ nN, $\Delta h \sim 0.2$ nm. Thus, the theoretical standard deviation of slip length $\Delta l_s = |\frac{\partial l_s}{\partial F_h}\Delta F_h + \frac{\partial l_s}{\partial h}\Delta h| = -\frac{6\pi R^2 \mu v}{F_h^2}\Delta F_h - \Delta h$. In our experiments, the separation chosen for fitting is < 200 nm, with corresponding $F_h > 2$ nN and $v < 100$ μm/s, then Δl_s is calculated and $\Delta l_s < 0.7$ nm. It should be noted that Δl_s is the limit of the accuracy, usually, the error bar of experiments $\Delta l_s^{exp.} \geq \Delta l_s$ because of the inherent randomness.

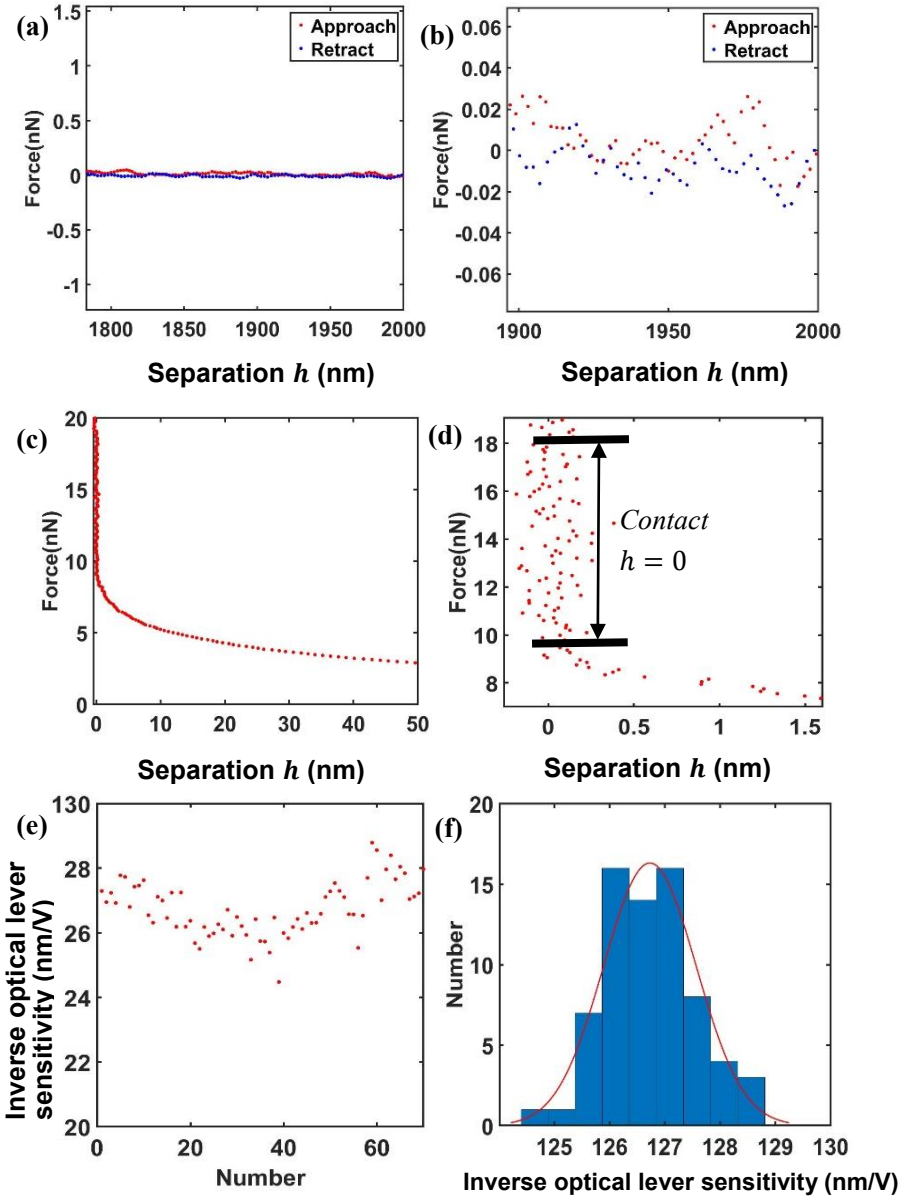

Figure S4. Factors influencing the accuracy of slip length measurement(a) Force curve of the far-end, the slop is approximately 0, meaning there is no obvious virtual deflection. (b) Enlarged view of Figure S4a, the peak-to-valley value is about 0.4 nN, reflecting the thermal noise, with corresponding RMS error $\Delta F_h \sim 0.01$ nN. (c) Force curve near the contact region. (d) Enlarged view of Figure S4c, the amplitude of the vibration means the peak-to-valley error of contact point is below 1 nm, with corresponding root-mean-square error <0.2 nm; (e) Inverse optical lever sensitivity values of 70 force curves of single-layer graphene on silica

measured in the same location, the amplitude is < 1 nm, indicating the relative error is ~ 1%; (f) The Gauss fit distribution of Figure S4e, the fitting result is 126.7±0.84 nm/V, and the relative error is <1%.

5. Materials characterization

5.1 1, 2, 3-layer graphene on SiO_2

The graphene samples are characterized by optical microscope, AFM and Raman spectrum respectively.

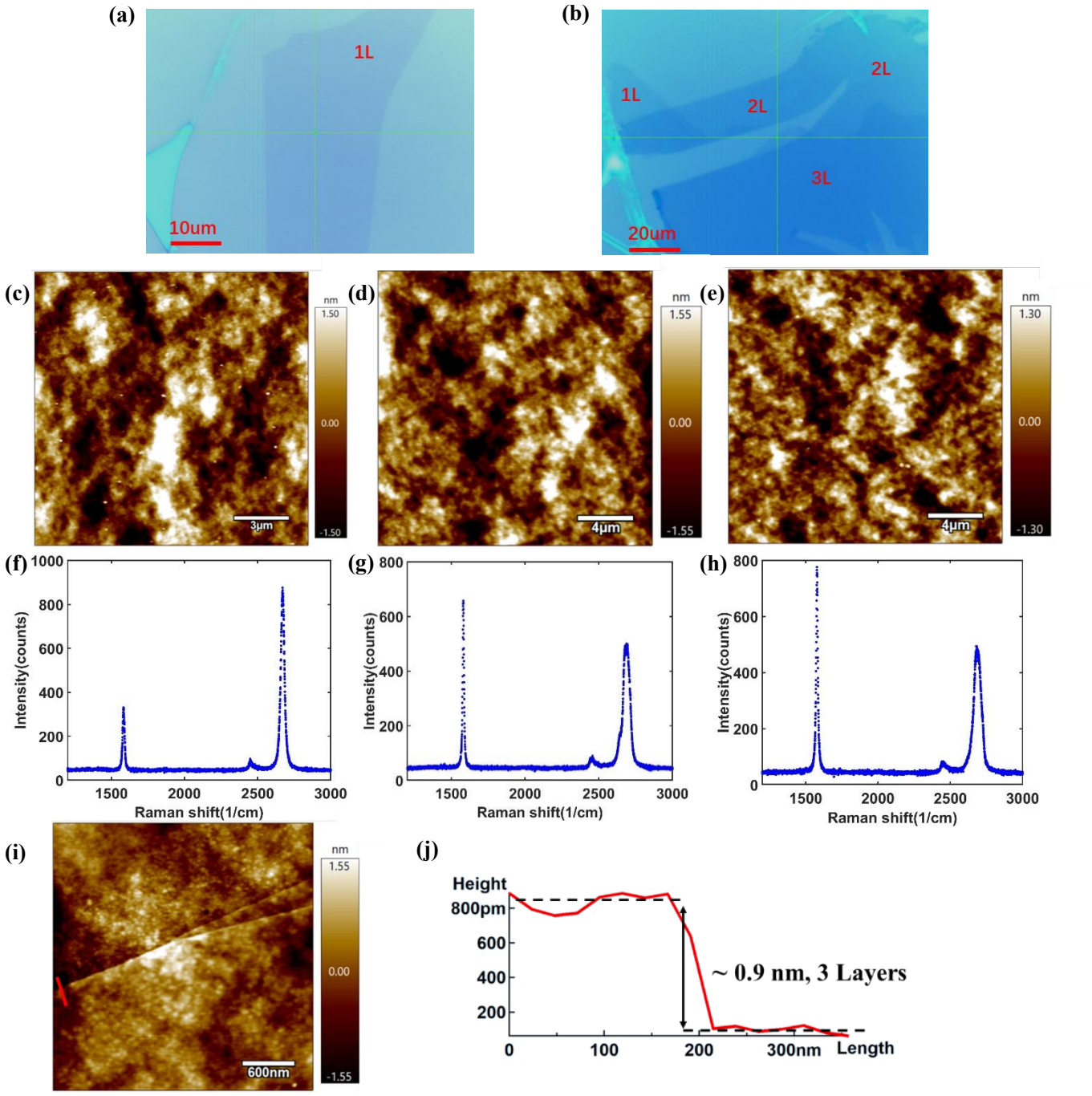

Figure S5. Characterization of 1, 2, 3-layer graphene on SiO_2. (a, b): Optical images of 1, 2, 3-layer graphene on SiO_2. (c, d, e):AFM morphology of 1, 2, 3-layer graphene on SiO_2 respectively. (f, g, h): Raman spectrum results of 1, 2, 3-layer graphene on SiO_2 respectively. (i): AFM morphology of the step of 3-layer graphene on SiO_2. (j): The step height along the red line in Figure S5i, the height is about 0.9 nm, corresponding to 3 layers thick.

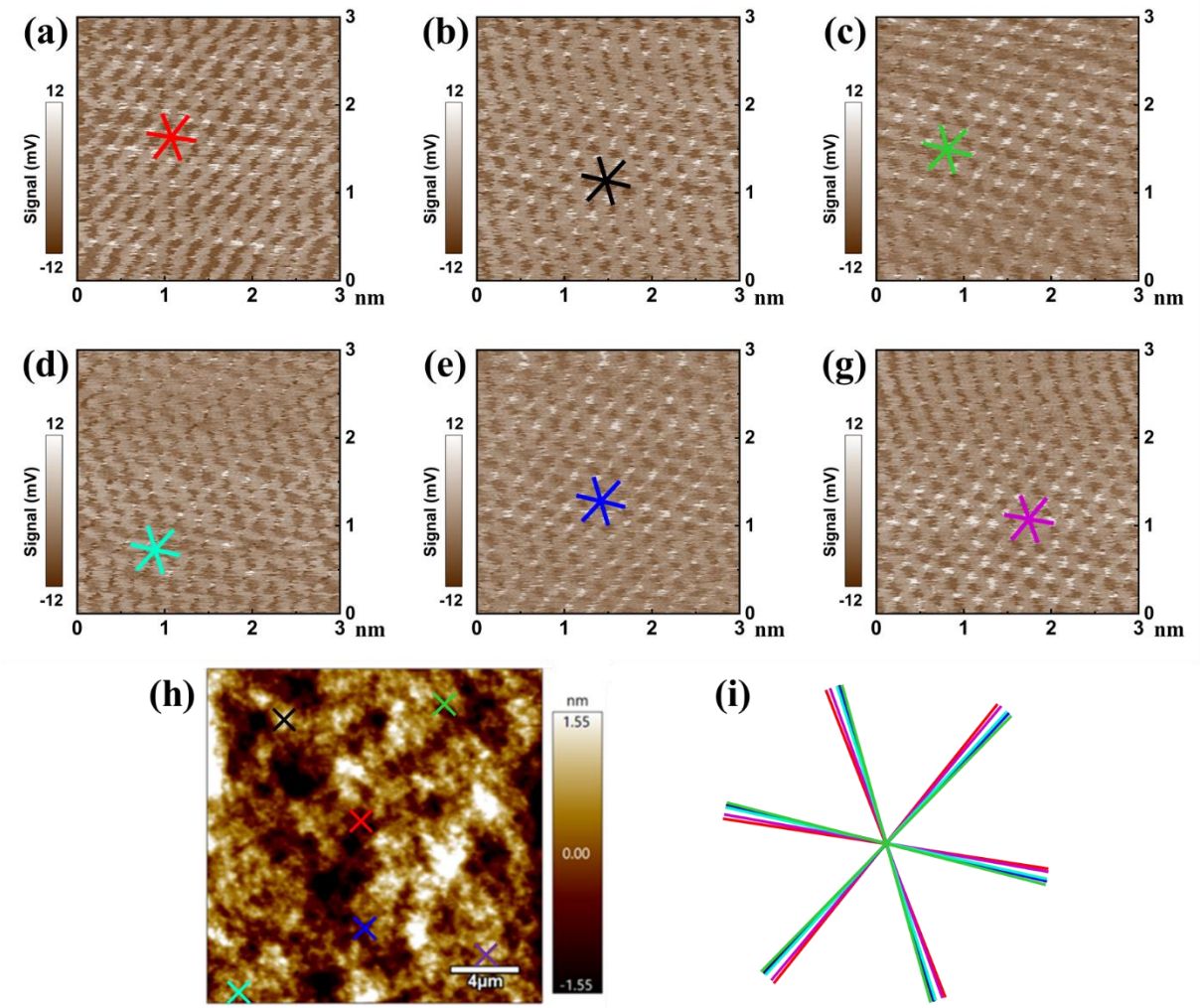

Figure S6. Atomic images of 2-layer graphene supported by SiO_2. (a~g) Atomic images of graphene at different locations, the snowflakes indicate the lattice direction. (h) Approximate measurement locations for Figure S6 a~g. (i) Lattice directions of Figure S6 a~g, the similar lattice directions indicate the single crystal property of graphene.

5.2 4, 6-layer graphene on silica

For FLG with thickness larger than 3 layers, the Raman spectrum is hard to be used for the characterization of layer numbers. Therefore, the graphene samples are characterized by optical microscope, AFM respectively.

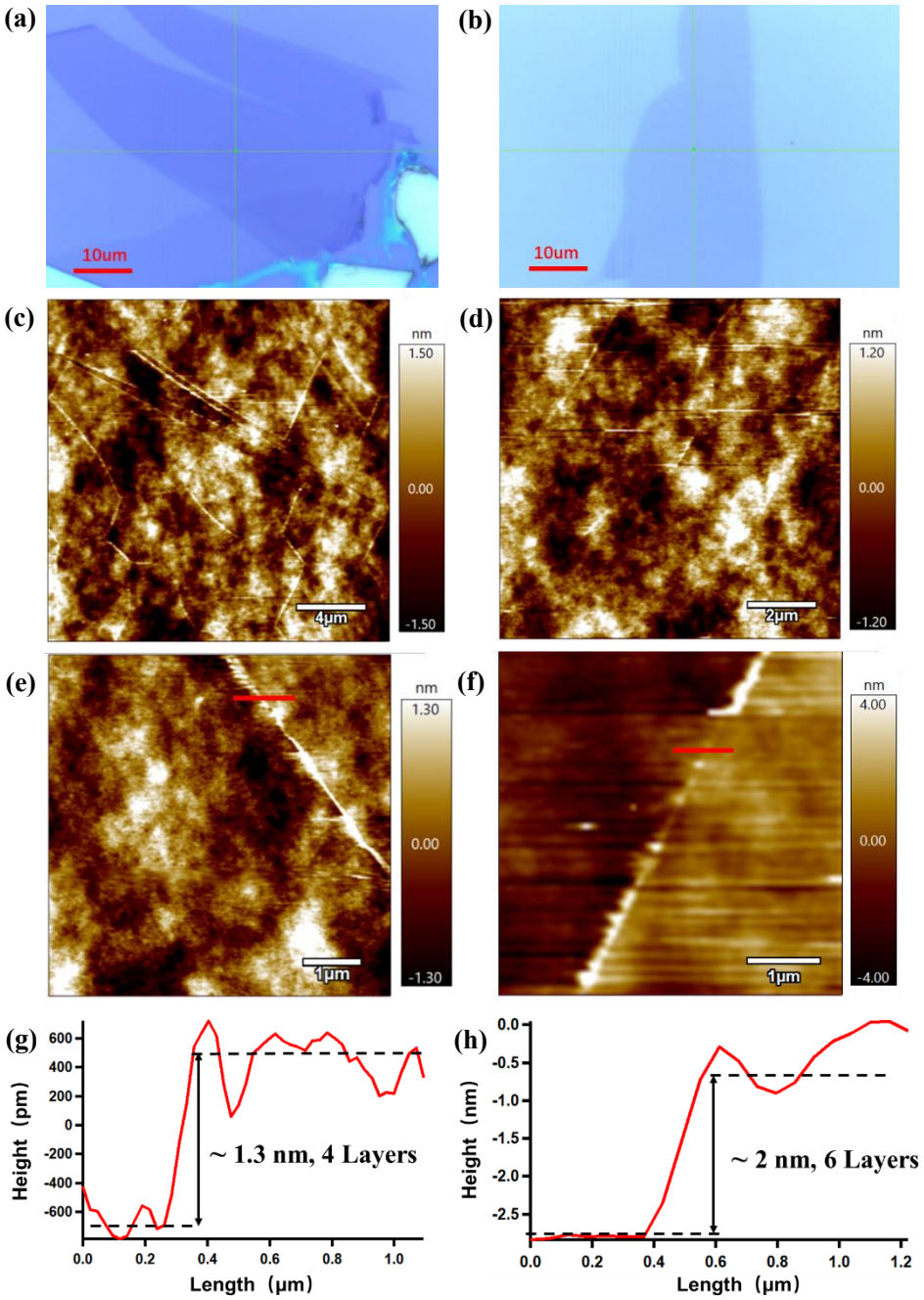

Figure S7. Characterization of 4, 6-layer graphene on SiO_2. (a, b): Optical images of 4, 6-layer graphene on SiO_2 respectively. (c, d):AFM morphology of 4, 6-layer graphene on SiO_2 respectively. (e, f): AFM morphology of the step of 4, 6-layer graphene on SiO_2 respectively. (g, h): the step height along the red line in Figure S7e, f, the height is about 1.3 nm and 2 nm, corresponding to 4 and 6 layers thick respectively.

5.3 1, 2-layer graphene on OTS

The graphene samples are characterized by optical microscope, AFM and Raman spectrum respectively.

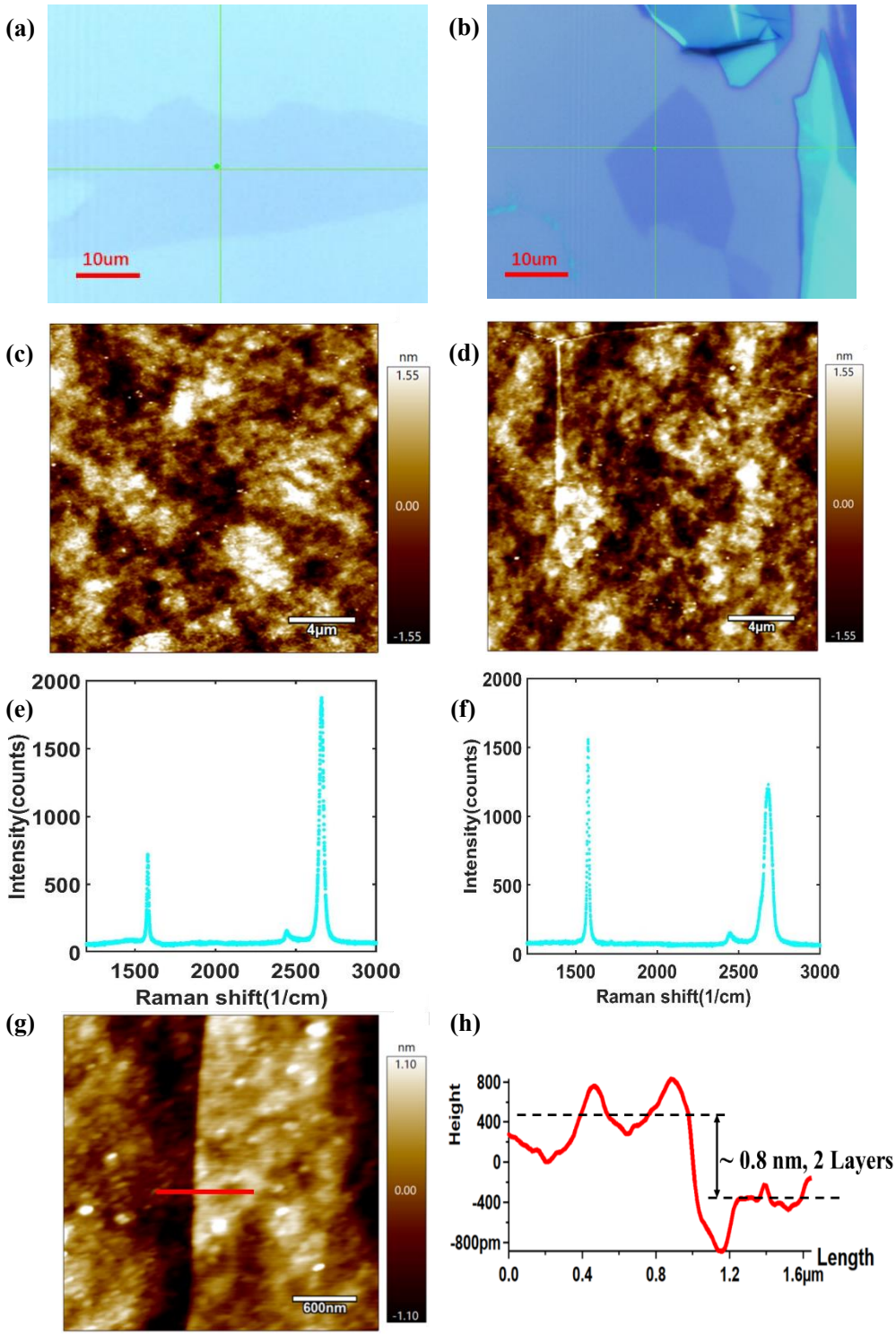

Figure S8. Characterization of 1, 2-layer graphene on OTS. (a, b): Optical images of 1, 2-layer graphene on OTS respectively. (c, d):AFM morphology of 1, 2-layer graphene on OTS respectively. (e, f): Raman spectrum of 1, 2-layer graphene on OTS respectively. (g): AFM morphology of the step of 2-layer graphene on OTS. (h): The step height along the red line in Figure S8g, the height is about 0.8 nm, corresponding to 2 layers thick. Figure S8 f and h strictly prove the 2 layers thick.

5.4 5, 9-layer graphene on OTS:

The graphene samples are characterized by optical microscope, AFM and Raman spectrum respectively.

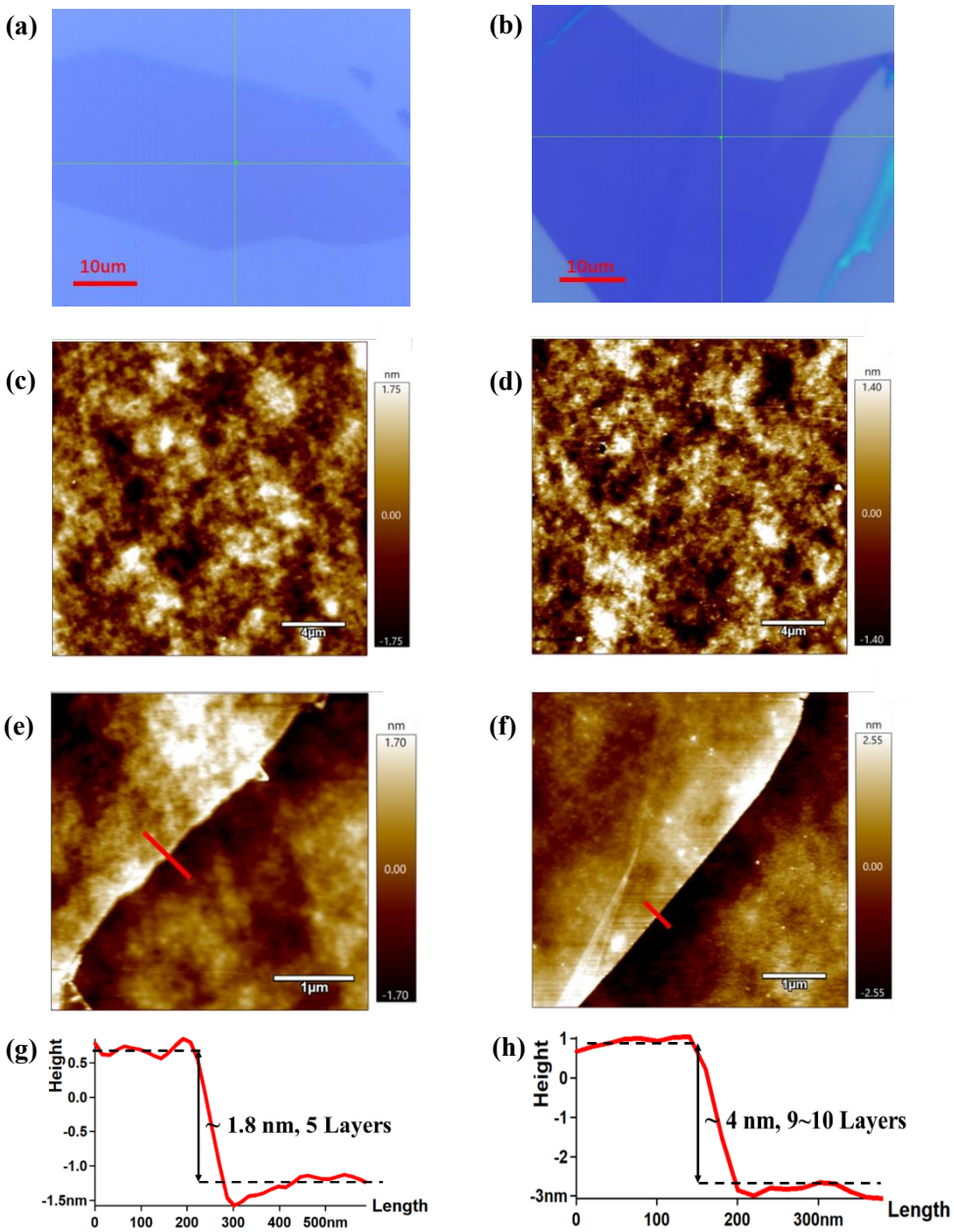

Figure S9. Characterization of 5, 9-layer graphene on OTS. (a, b): Optical images of 5, 9-layer graphene on OTS respectively. (c, d):AFM morphology of 5, 9-layer graphene on OTS respectively. (e, f): AFM morphology of the step of 5, 9-layer graphene on OTS. (g, h): The step height along the red line in Figure S9 e, f, the height is about 1.8 nm and 4 nm, corresponding to 5 and 9~10 layers thick. For graphene with thickness larger than 5 layers, there is about 1~2 layers error for the thickness estimation.

5.5 Colloidal probe characterization

The colloidal probe is characterized by scanning electron microscope (SEM) and AFM. The AFM morphology is measured by inverse imaging method based on a TGT1 standard sample (NT-MDT

instruments).[13] Red box is the area for zoom-scanning (400×400 nm^2). The RMS roughness for 400×400 nm^2 area is 0.5 nm. The inverse imaging of colloidal probe is a standard method, which can refer to the literature[13-15].

In view of the previous report that the probe may introduce a constant systematic error for slip length measurement due to tip roughness[16], cantilever shape[17] and stiffness[18], before each measurement on FLG, we first measure the apparent slip length on mica whose true slip length is zero, and we subtract the apparent slip length on mica from the slip length on FLG to exclude effect of the probe on the slip length measurement and get the true slip length.

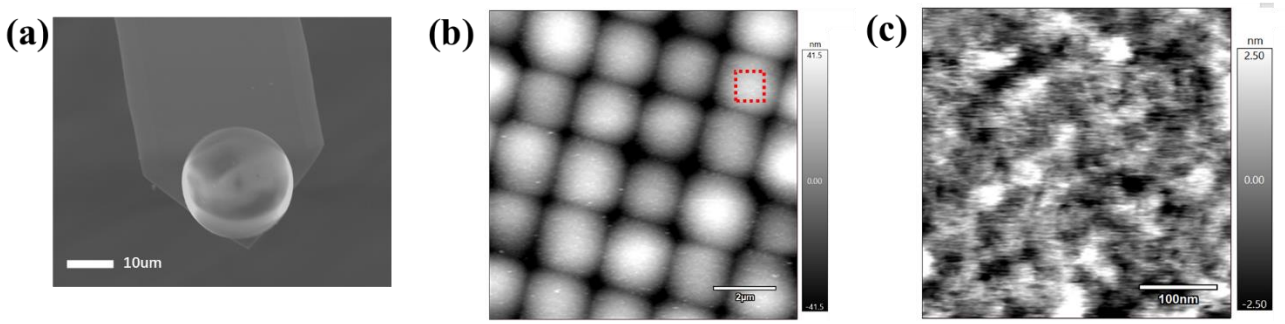

Figure S10. Characterization of colloidal probe. (a): SEM image of colloidal probe; (b) Inverse AFM morphology of colloidal probe; (c) zoomed morphology of red box in Figure S10b, the RMS roughness is about 1.2 nm.

5.6 Substrate characterization

Before graphene exfoliation, the substrates (SiO_2, OTS) are characterized by a contact angle measuring instrument. The contact angle for SiO_2 and OTS is 24.9° and 100.0° respectively.

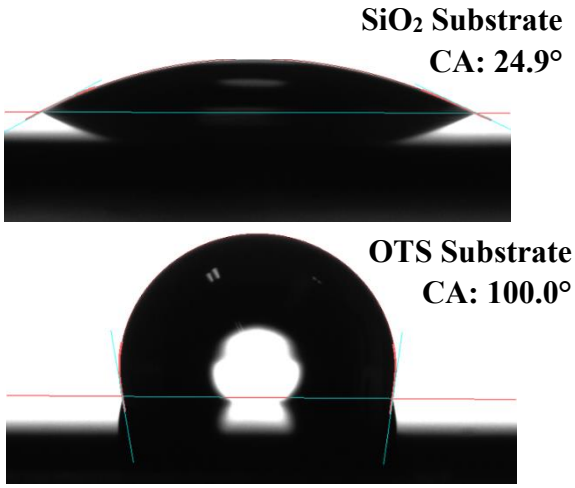

Figure S11. Contact angle (CA) of substrates.

6. Theoretical analysis details

6.1 Calculation of W_{ad} and scaling law

On molecular scale, the slip length is defined as $l_s = \eta/\lambda$, $\lambda = \frac{1}{Ak_{\mathrm{B}}T}\int_0^\infty \langle F_f(t)F_f(0)\rangle dt$ (Green-Kubo relation), where A is the contact area between liquid and solid, k_{B} is the Boltzmann constant, T is absolute temperature, $F_f(t)$ is friction force at time t. C. Sender and L. Bocquet et al. get an analytical approximate relation of friction coefficient[10, 19]

$$\lambda = \frac{1}{Ak_{\mathrm{B}}T}\int_0^\infty \langle F_f(t)F_f(0)\rangle dt \approx \frac{1}{Ak_{\mathrm{B}}T}\langle F_f^2\rangle \times t_0 \tag{S6.1}$$

where t_0 is the force autocorrelation time, $t_0 = \int_0^\infty \langle F_f(t)F_f(0)\rangle / \langle F_f^2\rangle \, dt$, and $t_0 \sim \sigma^2/D$, $\langle F_f^2\rangle \sim C\rho\sigma(\varepsilon/\sigma)^2$, D is the diffusion coefficient, C is a factor related to the surface morphology, ρ is the density of liquid, σ is the characteristic length and ε is the typical liquid-solid potential energy coefficient. The slip length can be further expressed as[10, 19, 20]

$$l_{\mathrm{s}} \sim \frac{k_{\mathrm{B}}T\eta D}{C\rho\sigma\varepsilon^2} \tag{S6.2}$$

For the intermolecular interaction potential $w(r)$ with given form, $\varepsilon \propto w(r) \propto W_{\mathrm{ad}} \propto (1+\cos\theta)$, where W_{ad} is the adhesion energy and θ is the contact angle [10, 19, 20]. As a result, $l_{\mathrm{s}} \sim k_{\mathrm{B}}T\eta D/C\rho\sigma\varepsilon^2 \sim (1+\cos\theta)^{-2}$ with other variables unchanged, which gives the qualitative relation between slip length and contact angle, termed as "scaling law" in some research.

Inspired by the theoretical analysis of wetting translucency[21], and taking the experimental regimes of this paper into account, we assume the intermolecular interactions between solid surfaces and liquid are Lennard-Jones (LJ) potential, then:

$$w_{\mathrm{Cw}}(r) = 4\varepsilon_{\mathrm{Cw}}\left(\frac{\sigma_{\mathrm{Cw}}^{12}}{r^{12}} - \frac{\sigma_{\mathrm{Cw}}^{6}}{r^{6}}\right) \tag{S6.3}$$

$$w_{\mathrm{Sw}}(r) = 4\varepsilon_{\mathrm{Sw}}\left(\frac{\sigma_{\mathrm{Sw}}^{12}}{r^{12}} - \frac{\sigma_{\mathrm{Sw}}^{6}}{r^{6}}\right) \tag{S6.4}$$

Where $\varepsilon_{\mathrm{Cw}}$, $\varepsilon_{\mathrm{Sw}}$, σ_{Cw}, σ_{Sw} are the interaction parameters and characteristic lengths of carbon-water and substrate-water respectively. Based on the continuum assumption, the intermolecular interaction can be integrated to the single molecule-surface interaction:

$$V_{\mathrm{Gw}}(z) = \rho_{\mathrm{C}}\iint w_{\mathrm{Cw}}dS = 4\pi\rho_{\mathrm{C}}\varepsilon_{\mathrm{Cw}}\left(\frac{\sigma_{\mathrm{Cw}}^{12}}{5z^{10}} - \frac{\sigma_{\mathrm{Cw}}^{6}}{2z^{4}}\right) \tag{S6.5}$$

$$V_{\mathrm{Sw}}(z) = \rho_{\mathrm{S}} \iiint w_{\mathrm{Sw}} dV = 4\pi\rho_{\mathrm{S}}\varepsilon_{\mathrm{Sw}}\left(\frac{\sigma_{\mathrm{Sw}}^{12}}{45z^9} - \frac{\sigma_{\mathrm{Sw}}^{6}}{6z^3}\right) \quad (S6.6)$$

$V_{\mathrm{Gw}}(z)$ is the potential energy between single water molecule and an infinite single-layer graphene, while $V_{\mathrm{Sw}}(z)$ is the potential energy between single water molecule and an infinite substrate; ρ_{C}, ρ_{S} are the density of the atoms in graphene and substrate respectively. It should be noted that the ρ_{C} is the density per area, while ρ_{S} is the density per volume. According to formulas (S6.5) and (S6.6), the potential between a water molecule and a N-layer-graphene-coated surface $V_{\mathrm{NSw}}(z)$ can be calculated as:

$$\begin{aligned} V_{\mathrm{NSw}}(z) &= \sum_{i=0}^{N-1} V_{\mathrm{Gw}}(z + iz_0) + V_{\mathrm{Sw}}(z + Nz_0) \\ &= 4\pi\rho_{\mathrm{C}}\varepsilon_{\mathrm{Cw}}\left(\sum_{i=0}^{N-1}\frac{\sigma_{\mathrm{Cw}}^{12}}{5(z+iz_0)^{10}} - \sum_{i=0}^{N-1}\frac{\sigma_{\mathrm{Cw}}^{6}}{2(z+iz_0)^{4}}\right) \\ &\quad + 4\pi\rho_{\mathrm{S}}\varepsilon_{\mathrm{Sw}}\left(\frac{\sigma_{\mathrm{Sw}}^{12}}{45(z+Nz_0)^9} - \frac{\sigma_{\mathrm{Sw}}^{6}}{6(z+Nz_0)^3}\right) \end{aligned} \quad (S6.7)$$

$z_0 = 0.34$ nm, which is the thickness of single-layer graphene. Furthermore, the adhesion energy of N-layer-graphene-coated surface W_{ad} can be continuously estimated:

$$W_{\mathrm{ad}} = \int \rho_{\mathrm{w}}(z) V_{\mathrm{NSw}}(z) dz \quad (S6.8)$$

Where $\rho_{\mathrm{w}}(z)$ is the density distribution of water molecules, for the analytical convenience, we adopt similar approach[21] by ignoring the density oscillation caused by the solvation effect, and estimate the density by the Boltzmann distribution, that is $\rho_{\mathrm{w}}(z) = \rho_{\mathrm{w0}} e^{-V_{\mathrm{NSw}}(z)/k_{\mathrm{B}}T}$, where ρ_{w0} is the bulk density.

Based on the proportional relation $\varepsilon \propto w(r) \propto W_{\mathrm{ad}}$ and the formula (S6.2), (S6.7), and (S6.8), we can get $l_{\mathrm{s}} \sim 1/W_{\mathrm{ad}}^2 = \kappa/W_{\mathrm{ad}}^2$, with κ as a scaling factor. We perform a numerical calculation to estimate the effect of adhesion energy on slip length translucency, the results are shown in Figure S12a. The LJ parameters are chosen according to the literature whose regime is similar to us:[22] $\varepsilon_{\mathrm{Cw}} = 12$ meV, $\sigma_{\mathrm{Sw}} = \sigma_{\mathrm{Cw}} = 3.19$ Å, $\rho_{\mathrm{C}} = 4/(\sqrt{3}a^2)$, $a = 2.49$ Å, $\rho_{\mathrm{S}} = \rho_{\mathrm{C}}^{1.5}$; for hydrophilic substrate, $\varepsilon_{\mathrm{Sw}} = 22$ meV; for hydrophobic substrate, $\varepsilon_{\mathrm{Sw}} = 4$ meV.

6.2 Calculation of ΔE

The scaling law fails in explaining the temperature-dependent slip because the contact angle is temperature-independent[23] while the slip length is temperature-dependent[24, 25] in the measured range. Thus, we proposed another theoretical estimation. Recently, some theoretical works have claimed that the slip length may vary even if the contact angle keeps constant[26-28], and the energy barrier ΔE of water molecule

moving from one equilibrium location to its neighbor on the solid surface plays key role on the slip length variation in these researches[26-28]. From this point of view, we explore the slip length translucency mechanism from the perspective of ΔE.

As mentioned in section 6.1, the slip length has close relationship with the friction force F_f via Green-Kubo relation. According to K. Falk and L. Bocquet et al, if we assume that the first layer of water at the interface dominate the friction shear stress, then the rms friction force $\langle F_f^2 \rangle$ can be approximated as[29]:

$$\frac{\langle F_f^2 \rangle}{A} \cong \frac{1}{2}\rho_1[S_1(\boldsymbol{q}_+) + S_1(\boldsymbol{q}_-)](q_0 \Delta E)^2 \qquad (S6.9)$$

ρ_1 is the density of the first water layer, S_1 is the two-dimensional structure factor of the first water layer, and ΔE is the interfacial energy barrier. The $\boldsymbol{q}_\pm$ are the reciprocal lattice vectors of graphene: $\boldsymbol{q}_\pm = q_0(1/\sqrt{3}, \pm 1)$, $q_0 = 2\pi/(\sqrt{3}a_{\mathrm{C-C}})$. In consideration of the similar surface morphology properties of graphene surfaces with different thickness, $\langle F_f^2 \rangle \sim \Delta E^2$, and $l_s \sim 1/\lambda \sim 1/\langle F_f^2 \rangle \sim 1/\Delta E^2 = \kappa_E/\Delta E^2$, with κ_E as a scaling factor similar to above mentioned κ, indicating the relations between slip length and surface energy barrier. Similar to section 6.1, we also perform a numerical model to calculate the influence of interfacial potential energy barrier based on formula (S6.9).

For section 6.2, the ΔE is calculated as the following process:

First, export the hexagonal lattice model of graphene from molecular dynamic simulation software (LAMMPS here) and get the location coordinates (x_c, y_c, z_c) of carbon atoms, c is the serial number with c=1, 2, 3, 4……, N_c, N_c is the total number of carbon atoms.

Second, define the pairwise interaction between water molecule and solid atom, here the pairwise interaction is still the same 12-6 Lennard-Jones interaction as section 6.1 describes.

Third, define the motion trajectory (x_l, y_l, z_l) of single water molecule, x_l, y_l, z_l are rectangular coordinates for water at location l with l=1, 2, 3, 4……, N_l where N_l is the total number of water locations.

Fourth, calculate the total interaction potential energy $U(x_l, y_l, z_l)$ between single water molecule and the solid surface, for location j, $U(x_l, y_l, z_l) = \sum_{k=1}^{k=N_c} w(r_{lk})$, where r_{lk} is the distance between single water molecule and the k^{th} solid atom, $w(r)$ is the pairwise interaction, equivalent to $w_{Cw}(r)$ or $w_{Sw}(r)$ for consideration of carbon-water and substrate-water interaction respectively.

Fifth, calculate the equilibrium locations according to $\partial U/\partial x_l = \partial U/\partial y_l = \partial U/\partial z_l = 0$ and get ΔE from the equilibrium locations. The numerical calculation is achieved in MATLAB, the results of ΔE has been shown in Figure S12a.

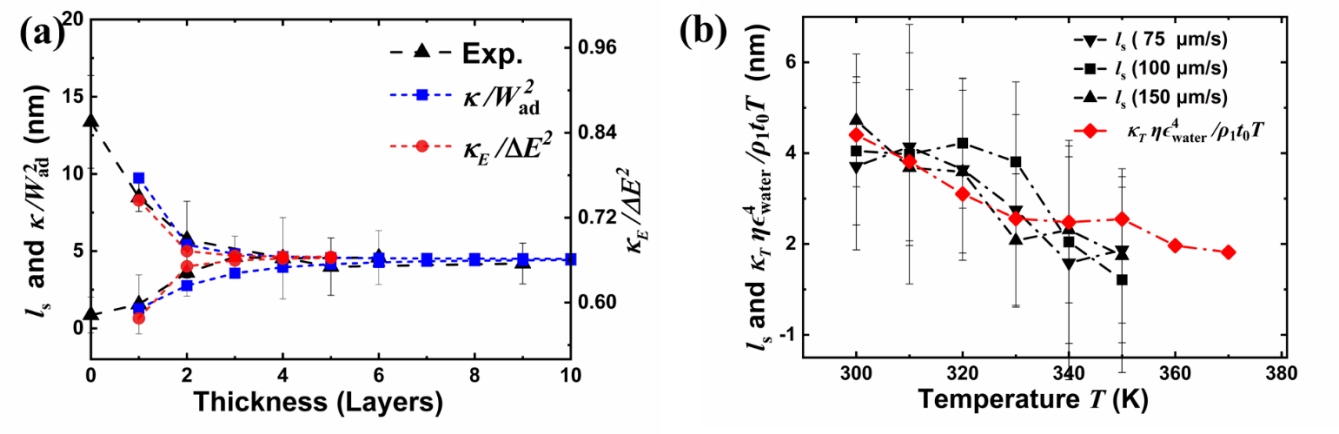

Figure S12. Theoretical explanation of slip length translucency and temperature dependence. (a) The agreement between l_s measured experimentally and estimated theoretically with either adhesion energy W_{ad} or energy barrier ΔE for FLG in different thickness. The fitted value for scaling factors κ and κ_E is 4.2×10^{-12} J/m and 2.0×10^{-42} J^2·nm respectively. (b) For 2-layer graphene on SiO_2, the comparison for l_s measured experimentally and estimated theoretically based on equation 2 at different temperature with different velocities v_{piezo}. The fitted value for scaling factor κ_T is 5.6×10^{-19} V^{4}m^{3}s^{2}K/C^4.

6.3 Effect of temperature: Combine McLachlan theory with ΔE Calculation

As mentioned above,ΔE is calculated from the linear additive water molecule-solid atom pairwise interaction $w(r)$ (12-6 Lennard-Jones for this paper), thus the temperature effect on the pairwise interaction directly affect ΔE, then affect the estimated slip length. Therefore, the key of temperature-dependent slip is the temperature-dependent pairwise interaction.

According to the McLachlan theory, the general pairwise attractive van der Waals interaction $w_{VDW}(r)$ between water molecule and solid atom in water medium can be expressed as[30, 31]

$$w_{VDW}(r) = -\frac{C_{VDW}}{r^6} = -\frac{6k_B T}{4\pi\epsilon_0 r^6}\left(\sum_{n=1}^{\infty}\frac{\alpha_w(i\nu_n)\alpha_c(i\nu_n)}{\epsilon_w^2(i\nu_n)} + \frac{1}{2}\frac{\alpha_w(i\nu_0)\alpha_c(i\nu_0)}{\epsilon_w^2(i\nu_0)}\right) \quad (S6.10)$$

where C_{VDW} is the coefficient of van der Waals potential, r is the distance between the water molecule and solid atom, ϵ_0 is the dielectric constant of vacuum, ϵ_w is the relative dielectric constant of the water medium, $\alpha_w(i\nu_n)$ and $\alpha_c(i\nu_n)$ are the polarizabilities of water molecule and carbon atom, expressed as $\alpha_w(i\nu_n) = \alpha_{w0}/[1 + i\Gamma_w(i\nu_n/\nu_{wI}) - (i\nu_n/\nu_{wI})^2]$, $\alpha_c(i\nu_n) = \alpha_{c0}/[1 + i\Gamma_c(i\nu_n/\nu_{cI}) - (i\nu_n/\nu_{cI})^2]$. α_{w0} and α_{c0} are the induced polarizabilities of water molecule and carbon atom,[31] $i\nu_n$ is the imaginary frequency of

molecules with i as the imaginary unit ($i^2 = -1$), n is the order of imaginary frequency being 0, 1, 2……, for simple polar molecules, $\nu_n = n(2\pi k_B T/\hbar) \cong 4n \times 10^{13}$ s^{-1} at 300 K, $\hbar$ is the Planck constant, Γ_w and Γ_c are coefficients, ν_{wI} and ν_{cI} are the adsorption frequencies (or the ionization frequencies) of the water molecule and solid atom. Typically, $\nu_{jI} \cong 3 \times 10^{15}$ s^{-1}. For water and carbon, Γ_w and $\Gamma_c \ll 1$, $(i\nu_n/\nu_{wI})^2$ and $(i\nu_n/\nu_{cI})^2 \ll 1$, thus $\alpha_w \cong \alpha_{w0}$, $\alpha_c \cong \alpha_{s0}$, being independent of T. [31]

The McLachlan theory explicitly shows the temperature effect on the attractive van der Waals interaction based on quantum mechanics. It indicates that the except for the temperature T, dielectric constant ϵ_w and polarizabilities α_w and α_c, may also change the van der Waals interaction[32]. For water and graphene, because α_w and α_s are nearly constant and independent of T. The dielectric constant of water is the main parameter that reflects the temperature effect on van der Waals interaction, $w_{VDW}(r) \sim T/\epsilon_w^2(\nu_n, T)$, here the dielectric constant of the water can be regarded as a function of both ν_n and T, because there is no external electromagnetic field in our experiments, thus the true frequency in our experiments is close to zero and has no effect on the dielectric property of water. As a result, the binary function $\epsilon_w(\nu_n, T)$ can be further simplified to a unary function $\epsilon_w(T)$ for our experiments. $w_{VDW}(r) \sim T/\epsilon_w^2(T)$ and the temperature dependence of ϵ_w on T at low frequency was solved by J. Bernal and R. Fowler[32].

For a 12-6 Lennard-Jones equilibrium system, the strength ratio of attractive interaction potential (6-order term, $w_{VDW}(r)$) to repulsive interaction potential (12-order term) is 2:1 at the equilibrium position[31]. Besides, considering the accurate analytical formula of the repulsive pairwise potential is still blank in quantum physics and there is still no report about the temperature dependence of the repulsive potential, we simply assume that in our focused temperature range (300~350 K), the pairwise interaction still follows the 12-6 Lennard-Jones form; in other words, the temperature-dependence of repulsive interaction is approximately close to the attractive one, thus, $w(r)$ is dominated by the attractive interaction $w_{VDW}(r)$, then $w(r) \sim T/\epsilon_w^2(T)$. Because ΔE is calculated from the extremum of the addition of the pairwise interaction, therefore $\Delta E \sim w(r) \sim w_{VDW}(r) \sim T/\epsilon_w^2(T)$. According to formula (S6.9), $\langle F_f^2 \rangle / A \cong \frac{1}{2}\rho_1[S_1(\boldsymbol{q}_+) + S_1(\boldsymbol{q}_-)](q_0 \Delta E)^2 \sim \rho_1[S_1(\boldsymbol{q}_+) + S_1(\boldsymbol{q}_-)]T^2/\epsilon_w^4(T)$, then $\lambda \approx \rho_1 t_0[S_1(\boldsymbol{q}_+) + S_1(\boldsymbol{q}_-)]T/k_B\epsilon_w^4(T)$. With MD simulations, C. Herrero and L. Joly et al found that the structure factors $S_1(\boldsymbol{q}_+)$ and $S_1(\boldsymbol{q}_-)$ are independent with temperature[24]. Finally, we have

$$l_s = \frac{\eta}{\lambda} = \kappa_T \frac{\eta \epsilon_w^4}{\rho_1 t_0 T}. \quad (S6.11)$$

It should be noted that for temperature-dependent slip length analysis, we just estimated the qualitative temperature dependence of ΔE on T based on McLachlan theory. There is no need to calculate ΔE directly as

section 6.2 for the temperature dependence because the temperature dependence of LJ parameters is unknown.

Then, according to discussion in the main text, all the temperature-dependent parameters, η, ϵ_w, ρ_1, t_0 can be calculated, then we calculate $\frac{\eta\epsilon_w^4}{\rho_1 t_0 T}$, fit the scaling factor κ_T, and compare it to the measured slip length, the comparison have been listed in the main text (Figure 4b in the main text and Figure S12b). The details of above parameters are listed as Table S1.

Table S1. The parameters used in formula (3) of the main text.

T (K)	300	310	320	330	340	350	360	370
η (mPa·s)	0.89	0.72	0.60	0.50	0.43	0.38	0.33	0.30
ϵ_w	78.3	74.8	71.5	68.3	65.3	62.4	59.7	57.0
ρ_1 (normalized)	1	0.85	0.73	0.64	0.56	0.49	0.43	0.39
t_0 ($\times 10^{-13}$s)	1.37	1.23	1.22	1.21	1.00	0.78	0.88	0.79

The data of η can refer to Ref. [33], and the data of ϵ_w can refer to Ref. [34]. The interfacial density ρ_1 was calculated by Boltzmann distribution as Ref. [21], and the force autocorrelation time t_0 was calculated by MD simulation as section 6.4 shows. Because the Boltzmann distribution may overestimate the interfacial density, we just did a normalization here.

6.4 MD simulation model for calculation of t_0

Molecular dynamics simulation was conducted to calculated the force relaxation time t_0 of water on SiO_2 supported double layer graphene. As shown in Figure S13, from top to bottom are the microsphere, water, double layer graphene, and amorphous SiO_2 respectively. The microsphere using in experiment is made of glass and mainly amorphous silica, thus was represented by an amorphous SiO_2 surface here in the simulations. The amorphous SiO_2 surface and substrate were both created from annealing [35], with a lateral size of 4.5 × 4.5 nm^2. The system was then packed with water molecules (a thickness of 3 nm) and two graphene layers in the middle of the SiO_2 surface and the SiO_2 substrate. CLAYFF force field [36] was used for both SiO_2 substrate and SiO_2 surface. SPC/E force field [37] was used for water molecules. The graphene sheets were modeled using the second-generation REBO potential [38], which is widely used for graphene. The interaction between water molecules and carbon atoms of graphene was modeled using the Lennard-Jones potential with

parameters from Ref. [39], with $\varepsilon_{CO} = 4.063$ meV and $\sigma_{CO} = 0.319$ nm. It corresponds to a contact angle θ of 86° for water on graphene. The interaction between the other molecules was described using the Lennard–Jones force field. Lorentz–Berthelot mixing rules were used for the inter-molecular interactions. Truncated and force-shifted LJ interaction that combines the standard Lennard-Jones function and subtracts a linear term based on the cutoff distance was used here [40], so that both, the potential and the force, go continuously to zero at the cutoff 1.2 nm. Long-range Columbic interactions were computed using the particle–particle particle–mesh (PPPM) algorithm. Periodic boundary conditions in all directions were implemented. All the MD simulations were carried out using a time step of 1 fs.

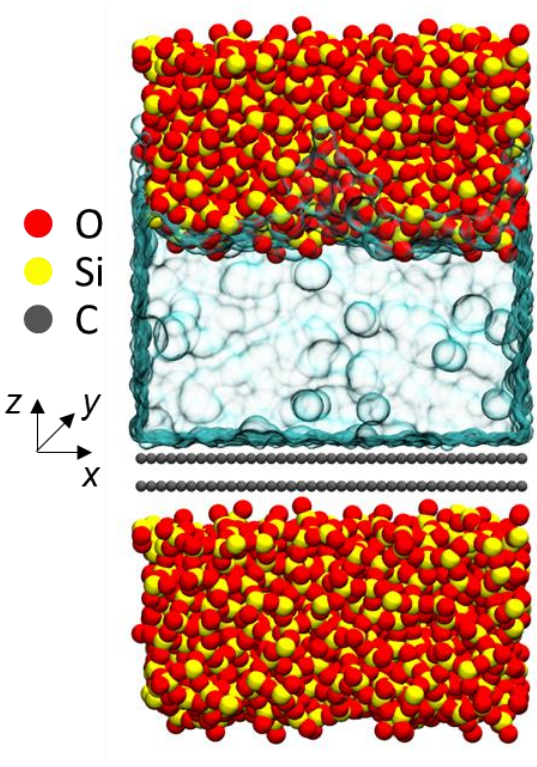

Figure S13. The side view of the MD simulation model.

During the simulations, the SiO_2 substrate was fixed, the top SiO_2 surface was constrained to move only in the *z* direction as a rigid body under a fixed normal pressure of 1 atm, as shown in Fig. S13. The water and graphene molecules were maintained at a temperature from 298 K to 368 K using Langevin thermostat. With the MD model, we calculated the force relaxation time [41] at different temperature as

$$t_0 = \int_0^\infty \frac{\langle F_x(t)F_x(0)\rangle}{\langle F_x^2\rangle} \mathrm{d}t\,, \tag{1}$$

where F_x is the force in x direction between water molecules and graphen-SiO_2 substrate and $\langle\ \rangle$ denotes the ensemble average at the equilibrium condition.

7. Velocity-independent slip length

In the main text, we mentioned that the slip length is independent of the velocity, here we list the details of slip length results on different samples at different piezo-velocity v_{piezo}. There is no obvious relevance between slip length and velocity.

Table S2: Slip length results on different samples at different piezo-velocity. (300 K)

Materials	v_{piezo}**(μm/s)**	**Number of curves**	**RMS (nm)**	l_s**(nm)**
SiO_2	150	80	0.719	0.9±1.2
HOPG	100	40	1.97	4.3±3.5
SLG/SiO_2	75	130	0.757	2.1±1.8
	100	130		1.3±2.1
	150	140		1.2±1.8
2-Layer FLG/SiO_2	75	60	0.765	3.2±1.8
	100	65		3.9±1.3
	150	90		3.7±1.4
3-Layer FLG/SiO_2	75	70	0.648	4.3±1.4
	100	60		4.7±1.2
	150	67		4.9±1.5
4-Layer FLG/SiO_2	75	70	0.745	4.4±2.1
	100	60		3.7±2.4
	150	79		5.4±3.5
6-Layer FLG/SiO_2	75	130	0.611	5.0±2.2
	100	130		4.4±2.0
	150	115		4.2±2.2
OTS	50	26	0.710	14.8±3.3
	75	13		12.8±3.1
	150	14		12.5±2.6
SLG/OTS	75	144	0.770	6.2±2.0
	100	133		10.2±4.0

	150	136		8.0±1.5
2-Layer				
FLG/OTS	75	75	0.776	5.7±1.0
	100	70		5.6±1.0
	150	75		5.9±0.7
5-Layer				
FLG/OTS	75	150	0.732	3.5±2.1
	100	145		5.0±2.3
	150	153		3.5±1.2
9-Layer				
FLG/OTS	75	60	0.707	4.1±1.5
	100	80		4.6±1.4
	150	75		3.8±1.1

8. Comparison with literature

8.1 Overall comparison

We list previous relevant experiments about water slip length on carbonous materials and compare our results with them as **Table S3**. Several groups have done water slip length measurement on graphite, and got the value of 4.5±4.4 nm[5] and 8±2 nm[7] respectively. The small difference can be attributed to the error from surface morphology of graphite, which contains many small steps with 1~10 nm height[1]. On graphene, the surface morphology is determined by the substrate, which is ~0.7 nm RMS for 20×20 μm^2 in our experiments, and the influence of the steps can be avoided. Quantitively, our converged results agree with the previous reports, indicating the correctness of the previous reports.

Together with the existing results in CNTs[42, 43], our slip length results of graphene is much smaller than the slip length in CNTs, validating the existing theoretical analysis about the curvature effect on slip where the slip length decreases with the radius of CNTs increasing[29].

Together with the and graphite/graphite nano-fluidics[44-46], an interesting phenomenon is observed. That is the slip length measured in nanochannels is much higher than in AFM and SFA. [4, 5, 7, 47-53] For example, the reported slip length in nanochannels (50~60 nm for graphite nanochannels with height 2~50 nm[45, 54], 16 nm for graphene nanochannels with height 40~100 nm[46]) is much larger than that measured in AFM (4.3±3.5 nm for HOPG and 1.6±1.9 nm for SLG on SiO_2 measured here, 4.5±4.4 nm[5] and 8 nm[7, 55] for

the literature). Furthermore, the slip length of water measured in graphite nanochannels (50~60 nm[20-21]) is even higher than on some smooth hydrophobic surfaces in AFM and SFA (15~30 nm, root-mean-square roughness < 1 nm[4, 47-53]), which is counterintuitive because the contact angle of graphite (70~80° [56, 57]) is less than those surfaces (~100°, typically[4, 47-53]) and the slip length is thought positively related to the contact angle[1, 19, 20]. Roughness and nanoconfinement are possible reasons for the counterintuitive results. Considering similar surface roughness (0.7 nm for FLG and 0.47~0.98 nm for graphene nanochannels[46]), this could be caused by the confinement of the nanochannels. However, the range (~50 nm) where confinement plays a role in slip length seems to be larger than previously thought (5 nm[45]).

Table S3. Previous experiments of water slip length on graphite/graphene surfaces.

Year	Authors	Materials	Methods	Slip length (nm)
2007	D. Honig and W. A. Ducker et al[5].	Graphite (HOPG) in open system (AFM)	experiments (AFM)	4.5±4.4
2008	A. Maali, H. Kellay et al.[7]	Graphite (HOPG) in open system (AFM)	experiments (AFM)	8±2
2013	D. Ortiz-Young et al.[58]	Graphite (HOPG) in open system (AFM)	experiments (AFM)	12.0±3.3 (overestimated), 6.8±2.9
2016	D. Li, Y. Pan and X. Zhao et al.[55]	Graphite (HOPG) in open system (AFM)	experiments (AFM)	~8
2016	E. Secchi, A. Siria and L. Bocquet et al.[42]	carbon nanotube (radius 15~50 nm)	experiments (nanofluidic)	300~20
2016 &2021	B. Radha, A. K Geim et al.[44, 45]	graphite nanochannels (height 1~30 nm)	experiments (nanofluidic) + MD	50~60 for experiments, ~50 for EMD and 80~100 for NEMD
2018	Q. Xie, H. G. Park, and C. Duan et al.[46]	graphene nanochannels (height ~50 nm)	experiments (nanofluidic)	0~200, the statical average is 16 nm fitted by lognormal distribution.
2021	Our results	SLG on SiO_2	experiments (AFM)	1.6±1.9
		SLG on OTS		8.5±0.9

6-layer FLG on SiO_2	4.6±1.7
9-layer FLG on OTS	4.2±1.3
HOPG	4.3±3.5

8.2 Discussion of D. Ortiz-Young et al's overestimation

In the work of D. Ortiz-Young et al, they measured the viscous shear force in nanoconfined water, and proposed new models to estimate the interfacial viscosity and slip length. Based on their *viscous force model*, they estimated the l_s of water on HOPG to be 12.0±3.3 nm, which is significantly different with our results. By examining the details of their estimation method, however, we found that the 12.0 nm may be an overestimation. Here are the reasons.

First, we find that there is another estimation method in D. Ortiz-Young's report[58]. Based on *tip energy dissipation model*, they estimated that the l_s of water on HOPG is 6.8±2.9 nm (Figure 4a and Supplementary Table S3 of their paper[58]), which is quite close to our results (4.3±3.5 nm) and the literatures we cited (4.5 ±4.4 nm[5], and 8 nm[7, 55]).

Second, their estimation where $l_s = 12.0$ nm for HOPG is based on *viscous force model*. This model relies on an assumption where the viscosities of interfacial water are the same on surfaces with different wettability and slip length. However, such assumption may be invalid. For example, K. Wu et al reviewed the series of existing calculated interfacial water viscosities μ_i and found that μ_i may be a function of surface contact angle, $\eta_i/\eta_\infty = -0.018\theta + 3.25$, where η_∞ is the bulk viscosity[59, 60]. Similar results were also reported by D. Feng et al[61] and H. Wang et al[62]. The common view of these researches is that lower contact angle lead to higher interfacial water viscosity[59-62].

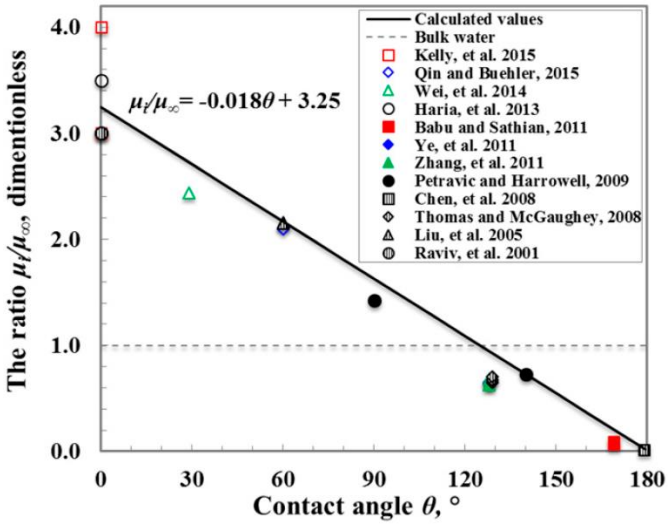

Figure S14. The dependence of interfacial water viscosity on wettability[59].

Third, if we consider the above discussions together, we will find that the 12.9 nm is an overestimation. In D. Ortiz-Young's *viscous shear force model,* they calculated slip length by the formula: $\frac{F_{shear}^{l_s}}{F_{shear}^{l_s=0}} = \frac{\eta^B(d)}{\eta^A(d)}\frac{d}{d+l_s}$, where $F_{shear}^{l_s}$ and η^B are the measured shear force and interfacial viscosity on surface where $l_s \neq 0$ respectively, while $F_{shear}^{l_s=0}$ and η^A are the measured shear force and interfacial viscosity on surface where $l_s = 0$ respectively. Such formula can be simply transformed as: $\frac{d+l_s}{d} = \frac{F_{shear}^{l_s=0}}{F_{shear}^{l_s}}\frac{\eta^B}{\eta^A}$. In D. Ortiz-Young et al's estimation, they assume $\frac{\eta^B}{\eta^A} = 1$. However, according to the above-mentioned studies[59-62], $\frac{\eta^B}{\eta^A} < 1$ actually. Thus, D. Ortiz-Young et al overestimated $\frac{\eta^B}{\eta^A}$ in their estimation where they thought $l_s = 12.9$ nm, and finally overestimated the slip length of water on HOPG.

Therefore, we can conclude that the 12.0 nm of l_s for water on HOPG is indeed an overestimation. But their measured 6.8 nm is a reasonable value, and close to our reports (4.3±3.5 nm).

9. The statistical analysis for temperature dependence results

The error bar in our experiments is about 1~2 nm. Even though this is a quite small error bar compared with that in other literatures[1, 7, 8, 17, 48, 49, 55, 58, 63-65], it is still large due to the small slip length. To further confirm the existence of temperature effect, we did a regression analysis.

We calculate the Pearson correlation coefficient (Pearson's r) of the measured temperature dependent experimental results, and the error was directly weighed. The range of Pearson's r is [−1, 1], where −1 and 1 means strict linear relation. The closer the absolute value of the Pearson's r is to 1, the stronger the l_s~T

correlation is. Here, for the results in Figure 2b and 4b in the main text, the Pearson's $r = -0.90$, indicating a strong negative correlation between slip length and temperature[66, 67], even within the consideration of error. Figure S15 gives the schematic of different Pearson correlation coefficients.

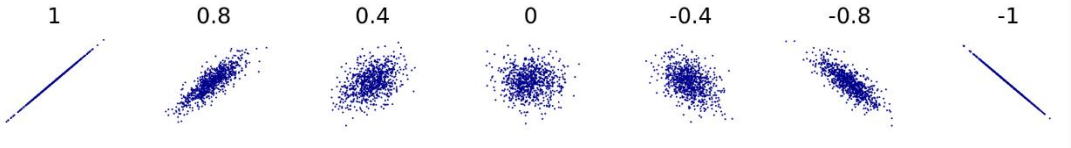

Figure S15. Schematics of different *r*. https://en.wikipedia.org/wiki/Pearson_correlation_coefficient

10. Gauss distribution of slip length results

For micro- and nanoscale measurement, the error is always worth to be taken good care of. We have performed detailed error analysis in the above sections. The actual measured results usually follow a distribution due to the thermal fluctuation, which requires repeated measurements. Here, every slip length reported in our main text is estimated based on an ensemble composed of at least 50 repeated measurements to ensure a Gauss distribution with the standard error being the error bar. For example, as Figure S16 shows, the slip length results of SLG/OTS follow a Gauss distribution where the average is 8.0 nm and the standard error is 1.5 nm, i.e., l_s= 8.0±1.5 nm.

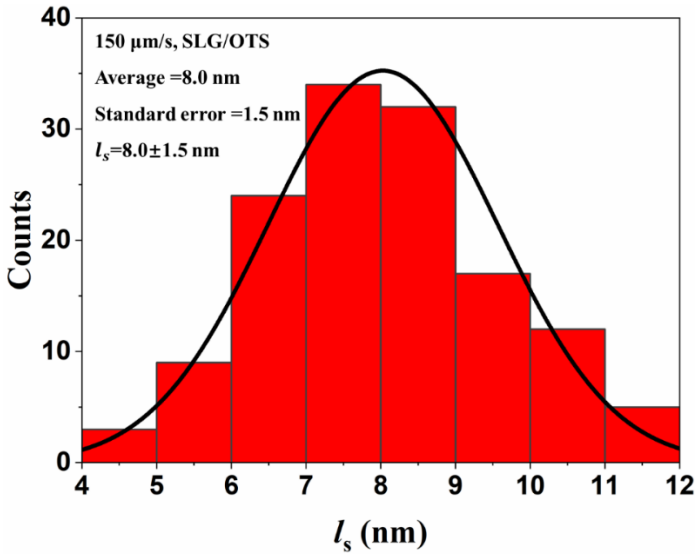

Figure S16. Gauss distribution of l_s for SLG/OTS based on 136 independent measurements.

11. Discussion about the electronic effect and quantum friction

For the electronic effect on nanofluidics, this is indeed an interesting question. Recently, the group of L. Bocquet et al has proposed a quantum friction theory where the electronic effect of liquid-solid interface is considered to influence the slippage[68]. This theory is based on the permutation theory and Keldysh

framework. The friction coefficient λ is divided to two parts, the classical parts λ_{Cl} and quantum part λ_Q. The quantum part λ_Q originates from the coupling of charge fluctuations in the liquid to electronic excitations in the solid. We tried to compare our results with the quantum friction theory. However, due to the limitation of present theory[68], only qualitative agreement for multilayer graphene can be established as discussed below.

In the quantum friction theory, $\lambda = \lambda_{Cl} + \lambda_Q$, where:

$$\lambda_{Cl} = \frac{1}{4\pi^2 k_B T} \int \mathrm{d}\mathbf{q}\, (\mathbf{q}\cdot\mathbf{v})^2/v^2\, |V_e(\mathbf{q})|^2 \int_0^{+\infty} dt S_w(\mathbf{q},t)$$

$$v \times \lambda_Q = \frac{1}{8\pi^2} \int_0^{+\infty} q dq(\hbar q) \int_0^{+\infty} \frac{d(\hbar\omega)}{k_B T} \frac{qv}{\sinh^2\left(\frac{\hbar\omega}{2k_B T}\right)} \times \frac{Im[g_e(q,\omega)]Im[g_w(q,\omega)]}{|1 - g_e(q,\omega)g_w(q,\omega)|^2}$$

$\mathbf{q}$ is wavevector with module q, $\mathbf{v}$ is velocity with module v, $V_e(\mathbf{q})$ is average Coulomb potential acting on the interfacial water layer, $S_w(\mathbf{q},t)$ is water charge structure factor, $g_e(q,\omega)$ is the surface response function for solid, $g_w(q,\omega)$ is the surface response function for water, ω is frequency.

Generally, the forms of g_e, g_w are complicated, but for bare (also called suspended) graphene and graphite, they can be simplified, then λ_{Cl} and λ_Q can be further theoretically calculated. The details of this calculation can referred to the Ref. [68] and its SI, and it will not be discussed here. According to the discussion by L. Bocquet et al, the quantum effect λ_Q on bare monolayer graphene is small, while on bare multilayer graphene or graphite is notable. By this theory, the quantum friction originating from the electronic effect was evaluated. For monolayer graphene, $\lambda_Q < 1\ \mathrm{Nsm^{-3}}$ and for multilayer graphene or graphite, λ_Q is $0.4 \times 10^3 \sim 10^5\ \mathrm{Nsm^{-3}}$, typically, as shown in the following Figure S17 (i.e. Fig.4 for Ref. [68]).

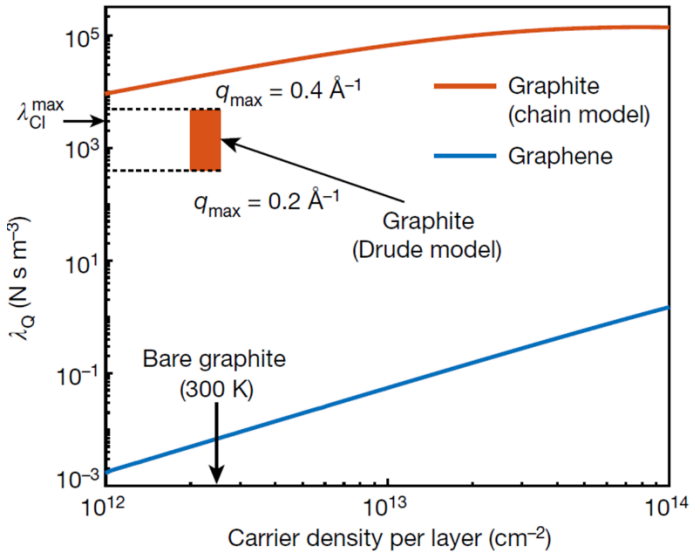

Figure S17. Quantum friction coefficient λ_Q for bare monolayer graphene and multilayer graphene (graphite) [68]

Besides, the total friction coefficient λ for bare monolayer and bare multilayer graphene is about $2 \times 10^4 \sim 10^5$ $\mathrm{Nsm^{-3}}$ and 3×10^3 $\mathrm{Nsm^{-3}}$ respectively. As a result, the quantum part λ_Q for bare monolayer graphene is neglectable, and for bare multilayer graphene is comparable to λ.

It should be noticed that the theoretical analysis in Ref. [68] didn't consider the effect of substrate, all the above discussions are for bare (also called suspended) monolayer and multilayer graphene. For multilayer graphene or graphite, the experimental measure l_s is about 4.3 nm here, corresponding $\lambda \cong 2 \times 10^5$ $\mathrm{Nsm^{-3}}$, consistent with the quantum friction theory. But for monolayer graphene, the theoretical estimation and experimental results are different. In the Ref. [68], the authors mentioned that the $\lambda = 3 \times 10^3$ $\mathrm{Nsm^{-3}}$ for monolayer graphene can be experimentally validated by the reports of Xie Q. et al[46], where l_s for graphene nanochannel is 200 nm, corresponding to $\lambda \cong 4.5 \times 10^3$ $\mathrm{Nsm^{-3}}$. However, such statement is loose. The 200 nm is a maximum slip length in Xie Q. et al.'s work[46], and the average l_s for graphene nanochannel is 16 nm, with a large error bar, as shown in Figure S18, corresponding to $\lambda = 6 \times 10^4$ $\mathrm{Nsm^{-3}}$. Our experiment shows that the slip length of monolayer graphene depends on the substrate, l_s is measured as 8.5 nm and 1.6 nm for monolayer graphene supported by OTS and SiO_2 respectively, corresponding to $\lambda \cong 1 \times 10^5$ and 6×10^5 $\mathrm{Nsm^{-3}}$ respectively. Therefore, for λ both Xie Q.'s results and ours are much larger than the theoretical estimated 3×10^3 $\mathrm{Nsm^{-3}}$ in the present quantum friction theory. In consideration that the graphene in both Xie Q.'s experiments and ours are both supported by substrates (SiO_2 for both and OTS for ours), it is reasonable to suppose that the substrate may have extra quantum effect on the liquid-solid friction of graphene, which leads to the difference between experimental results and theoretical estimation for monolayer graphene.

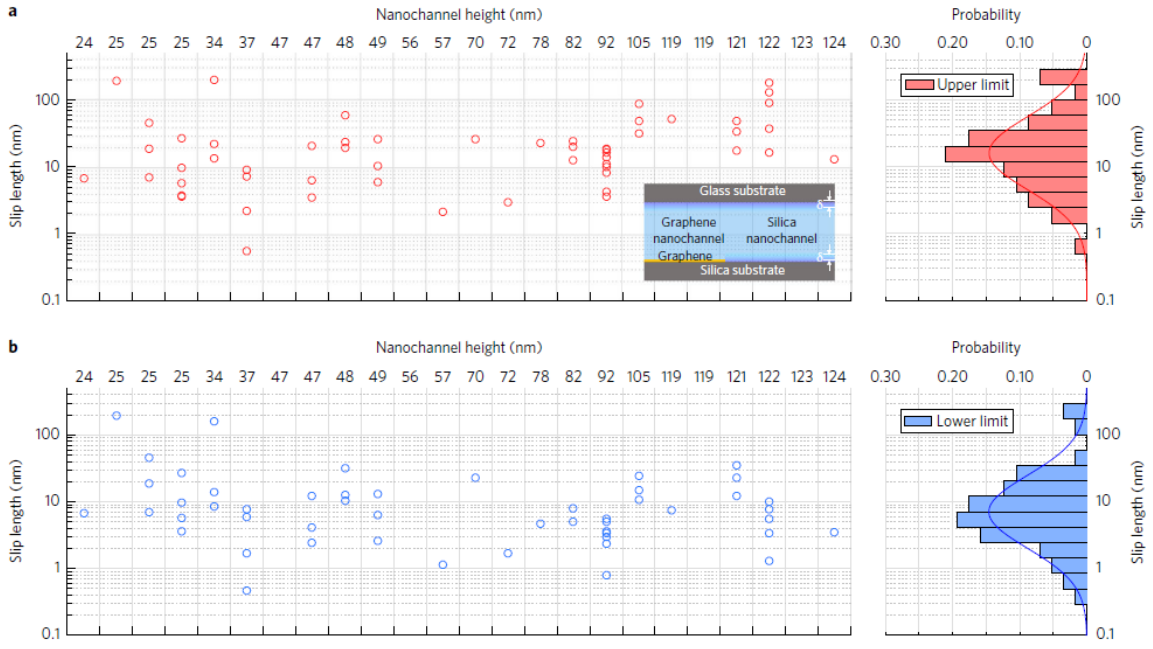

Figure S18. The slip length of water in graphene nanochannels reported by Xie Q. et al[46]. (a) The

extracted slip length considering graphene coverage/quality in the nanochannel. (b) The extracted slip length without considering graphene coverage/quality in the nanochannel.

As mentioned above, the calculations of λ_{Cl} and λ_Q need the information of $V_e(\mathbf{q})$, $S_w(\mathbf{q},t)$, $g_e(q,\omega)$, $g_w(q,\omega)$ et al. $V_e(\mathbf{q})$ and $S_w(\mathbf{q},t)$ are common-used in classical MD simulations, and easy to be obtained. However, $g_e(q,\omega)$ and $g_w(q,\omega)$ lack of reference. Due to the simple atomic lattice of graphene and graphite, $g_e(q,\omega)$ and $g_w(q,\omega)$ can be simplified and used for quantitative calculation, as in Ref. [68]. But the substrate we used here (SiO_2 and OTS) is more complicated than graphene and graphite, as a result, the corresponding $g_e(q,\omega)$ and $g_w(q,\omega)$ for supported graphene will change and become more complicated. Until now, the exact mathematical form of $g_e(q,\omega)$ and $g_w(q,\omega)$ for supported graphene is still unknown, thus λ_{Cl} and λ_Q for supported graphene cannot be calculated at present.

Except for the monolayer graphene, for our temperature dependence measurement on 2-layer graphene, the slip length is negative to the temperature. According to the quantum friction theory, the wavevector q_{max} will increase with temperature (q_{max} =0.2 Å^{-1} for 300 K and 0.4 Å^{-1} for 600 K), and then leads to the increase of λ_Q on multilayer graphene and graphite ($\lambda_Q = 0.4\times10^3$ Nsm^{-3} for q_{max} =0.2 Å^{-1}, and $\lambda_Q = 5\times10^3$ Nsm^{-3} for q_{max} =0.4 Å^{-1})[68]. Thus, our results are qualitatively consistent with the quantum friction theory. The negatively temperature dependent slip length can be attributed to the increase of the quantum friction factor λ_Q.

In summary, we noticed that the electronic effect may influence the slip length, which has been proposed as quantum friction theory by L. Bocquet. We compared our experimental results with the quantum friction theory. For monolayer graphene, we found a large difference between them. Such difference may originate from the quantum effect of substrate on liquid-solid friction. However, because the surface response functions of supported graphene is unknown and theoretically complicated, the electronic effect of supporting substrates on slip length cannot be solved at present. For multilayer graphene, our temperature dependent results are qualitatively consistent with quantum friction theory, the temperature dependence can be attributed to the increase of quantum friction factor λ_Q.

References

[1] T. Lee, E. Charrault, C. Neto, Interfacial slip on rough, patterned and soft surfaces: A review of experiments and simulations, Advances in Colloid and Interface Science, 210 (2014) 21-38.

[2] H.J. Butt, B. Cappella, M. Kappl, Force measurements with the atomic force microscope: Technique, interpretation and applications, Surf. Sci. Rep., 59 (2005) 1-152.

[3] O.I. Vinogradova, DRAINAGE OF A THIN LIQUID-FILM CONFINED BETWEEN HYDROPHOBIC SURFACES, Langmuir, 11

(1995) 2213-2220.
[4] C. Cottin-Bizonne, A. Steinberger, B. Cross, O. Raccurt, E. Charlaix, Nanohydrodynamics: The intrinsic flow boundary condition on smooth surfaces, Langmuir, 24 (2008) 1165-1172.
[5] C.D.F. Honig, W.A. Ducker, Thin film lubrication for large colloidal particles: Experimental test of the no-slip boundary condition, J. Phys. Chem. C, 111 (2007) 16300-16312.
[6] C.D.F. Honig, W.A. Ducker, No-slip hydrodynamic boundary condition for hydrophilic particles, Physical review letters, 98 (2007).
[7] A. Maali, T. Cohen-Bouhacina, H. Kellay, Measurement of the slip length of water flow on graphite surface, Appl. Phys. Lett., 92 (2008) 053101.
[8] L. Zhu, P. Attard, C. Neto, Reliable Measurements of Interfacial Slip by Colloid Probe Atomic Force Microscopy. II. Hydrodynamic Force Measurements, Langmuir, 27 (2011) 6712-6719.
[9] L. Wan, Y.M. Huang, Slip length of confined liquid with small roughness of solid-liquid interfaces, Physical Review E, 95 (2017) 043107.
[10] C. Sendner, D. Horinek, L. Bocquet, R.R. Netz, Interfacial Water at Hydrophobic and Hydrophilic Surfaces: Slip, Viscosity, and Diffusion, Langmuir, 25 (2009) 10768-10781.
[11] Y. Pan, B. Bhushan, A. Maali, Slip Length Measurement of Confined Air Flow on Three Smooth Surfaces, Langmuir, 29 (2013) 4298-4302.
[12] V.S.J. Craig, C. Neto, （61）In situ calibration of colloid probe cantilevers in force microscopy: Hydrodynamic drag on a sphere approaching a wall, Langmuir, 17 (2001) 6018-6022.
[13] C. Neto, V.S.J. Craig, Colloid probe characterization: Radius and roughness determination, Langmuir, 17 (2001) 2097-2099.
[14] P.J. van Zwol, G. Palasantzas, M. van de Schootbrugge, J.T.M. de Hosson, V.S.J. Craig, Roughness of microspheres for force measurements, Langmuir, 24 (2008) 7528-7531.
[15] L. Kain, O.G. Andriotis, P. Gruber, M. Frank, M. Markovic, D. Grech, V. Nedelkovski, M. Stolz, A. Ovsianikov, P.J. Thurner, Calibration of colloidal probes with atomic force microscopy for micromechanical assessment, Journal of the Mechanical Behavior of Biomedical Materials, 85 (2018) 225-236.
[16] O.I. Vinogradova, G.E. Yakubov, Surface roughness and hydrodynamic boundary conditions, Physical Review E, 73 (2006).
[17] C.L. Henry, V.S.J. Craig, Measurement of no-slip and slip boundary conditions in confined Newtonian fluids using atomic force microscopy, Phys. Chem. Chem. Phys., 11 (2009) 9514-9521.
[18] C.D.F. Honig, W.A. Ducker, Squeeze Film Lubrication in Silicone Oil: Experimental Test of the No-Slip Boundary Condition at Solid-Liquid Interfaces, J. Phys. Chem. C, 112 (2008) 17324-17330.
[19] L. Bocquet, E. Charlaix, Nanofluidics, from bulk to interfaces, Chem. Soc. Rev., 39 (2010) 1073-1095.
[20] N. Kavokine, R.R. Netz, L. Bocquet, Fluids at the Nanoscale: From Continuum to Subcontinuum Transport, Annual Review of Fluid Mechanics, Vol 53, 53 (2021) 377-410.
[21] C.-J. Shih, Q.H. Wang, S. Lin, K.-C. Park, Z. Jin, M.S. Strano, D. Blankschtein, Breakdown in the Wetting Transparency of Graphene, Physical review letters, 109 (2012) 176101.
[22] Y. Wang, Y. Guo, W. Guo, Screening effect of monolayer van der Waals crystals on surface deicing: a molecular simulation study, Phys. Chem. Chem. Phys., 22 (2020) 27873-27881.
[23] J.-W. Song, L.-W. Fan, Temperature dependence of the contact angle of water: A review of research progress, theoretical understanding, and implications for boiling heat transfer, Advances in colloid and interface science, 288 (2021) 102339-102339.
[24] C. Herrero, G. Tocci, S. Merabia, L. Joly, Fast increase of nanofluidic slip in supercooled water: the key role of dynamics, Nanoscale, 12 (2020) 20396-20403.
[25] K.L. Wu, Z.X. Chen, J. Li, J.Z. Xu, K. Wang, S.H. Wang, X.H. Dong, Z.Y. Zhu, Y. Peng, X.F. Jia, X.F. Li, Manipulating the Flow of Nanoconfined Water by Temperature Stimulation, Angewandte Chemie-International Edition, 57 (2018) 8432-8437.

[26] B. Ramos-Alvarado, S. Kumar, G.P. Peterson, Wettability transparency and the quasiuniversal relationship between hydrodynamic slip and contact angle, Appl. Phys. Lett., 108 (2016) 074105.
[27] Y.B. Xie, L. Fu, T. Niehaus, L. Joly, Liquid-Solid Slip on Charged Walls: The Dramatic Impact of Charge Distribution, Physical review letters, 125 (2020) 014501.
[28] C. Wang, H. Yang, X. Wang, C. Qi, M. Qu, N. Sheng, R. Wan, Y. Tu, G. Shi, Unexpected large impact of small charges on surface frictions with similar wetting properties, Communications Chemistry, 3 (2020) 27.
[29] K. Falk, F. Sedlmeier, L. Joly, R.R. Netz, L. Bocquet, Molecular Origin of Fast Water Transport in Carbon Nanotube Membranes: Superlubricity versus Curvature Dependent Friction, Nano Letters, 10 (2010) 4067-4073.
[30] A.D. McLachlan, RETARDED DISPERSION FORCES IN DIELECTRICS AT FINITE TEMPERATURES, Proceedings of the Royal Society of London Series a-Mathematical and Physical Sciences, 274 (1963) 80-+.
[31] J.N. Israelachvili, Intermolecular and Surface Forces, 3rd Edition, Intermolecular and Surface Forces, 3rd Edition, DOI (2011) 1-674.
[32] J.D. Bernal, R.H. Fowler, A theory of water and ionic solution, with particular reference to hydrogen and hydroxyl ions, Journal of Chemical Physics, 1 (1933) 515-548.
[33] H.E.K. Joseph Kestin, and Robert J. Correia, Tables of the dynamic and kinematic viscosity of aqueous NaCl solutions in the temperature range 20–150 °C and the pressure range 0.1–35 MPa, Journal of Physical and Chemical Reference Data, 10 (1981) 010071.
[34] A.A.M. C. G. Malmberg, Dielectric constant of water from 0 to 100 C, Journal of research of the National Bureau of Standards, 56 (1956) 1.
[35] R.G. Dellavalle, H.C. Andersen, MOLECULAR-DYNAMICS SIMULATION OF SILICA LIQUID AND GLASS, Journal of Chemical Physics, 97 (1992) 2682-2689.
[36] T.A. Ho, D. Argyris, D.V. Papavassiliou, A. Striolo, L.L. Lee, D.R. Cole, Interfacial water on crystalline silica: a comparative molecular dynamics simulation study, Mol. Simul., 37 (2011) 172-195.
[37] H.J.C. Berendsen, J.R. Grigera, T.P. Straatsma, THE MISSING TERM IN EFFECTIVE PAIR POTENTIALS, J. Phys. Chem., 91 (1987) 6269-6271.
[38] D.W. Brenner, O.A. Shenderova, J.A. Harrison, S.J. Stuart, B. Ni, S.B. Sinnott, A second-generation reactive empirical bond order (REBO) potential energy expression for hydrocarbons, J. Phys.-Condes. Matter, 14 (2002) 783-802.
[39] T. Werder, J.H. Walther, R.L. Jaffe, T. Halicioglu, P. Koumoutsakos, On the water-carbon interaction for use in molecular dynamics simulations of graphite and carbon nanotubes, J. Phys. Chem. B, 107 (2003) 1345-1352.
[40] S. Toxvaerd, J.C. Dyre, Communication: Shifted forces in molecular dynamics, Journal of Chemical Physics, 134 (2011).
[41] N. Wei, X.S. Peng, Z.P. Xu, Breakdown of fast water transport in graphene oxides, Phys. Rev. E, 89 (2014) 8.
[42] E. Secchi, S. Marbach, A. Nigues, D. Stein, A. Siria, L. Bocquet, Massive radius-dependent flow slippage in carbon nanotubes, Nature, 537 (2016) 210-213.
[43] S.K. Kannam, B.D. Todd, J.S. Hansen, P.J. Daivis, How fast does water flow in carbon nanotubes?, Journal of Chemical Physics, 138 (2013) 094701.
[44] B. Radha, A. Esfandiar, F.C. Wang, A.P. Rooney, K. Gopinadhan, A. Keerthi, A. Mishchenko, A. Janardanan, P. Blake, L. Fumagalli, M. Lozada-Hidalgo, S. Garaj, S.J. Haigh, I.V. Grigorieva, H.A. Wu, A.K. Geim, Molecular transport through capillaries made with atomic-scale precision, Nature, 538 (2016) 222-+.
[45] A. Keerthi, S. Goutham, Y. You, P. Iamprasertkun, R.A.W. Dryfe, A.K. Geim, B. Radha, Water friction in nanofluidic channels made from two-dimensional crystals, Nature communications, 12 (2021) 3092.
[46] Q. Xie, M.A. Alibakhshi, S.P. Jiao, Z.P. Xu, M. Hempel, J. Kong, H.G. Park, C.H. Duan, Fast water transport in graphene nanofluidic channels, Nature nanotechnology, 13 (2018) 238-+.
[47] A.P. Bowles, W.A. Ducker, Flow of Water Adjacent to Smooth Hydrophobic Solids, J. Phys. Chem. C, 117 (2013) 14007-14013.
[48] Y.L. Pan, B. Bhushan, Role of surface charge on boundary slip in fluid flow, Journal of Colloid and Interface Science, 392 (2013) 117-121.

[49] Y. Lia, B. Bhushan, The effect of surface charge on the boundary slip of various oleophilic/phobic surfaces immersed in liquids, Soft Matter, 11 (2015) 7680-7695.
[50] J. Heverhagen, M. Tasinkevych, A. Rahman, C.T. Black, A. Checco, Slip Length Enhancement in Nanofluidic Flow using Nanotextured Superhydrophobic Surfaces, Advanced Materials Interfaces, 3 (2016).
[51] Y.X. Zhu, S. Granick, Rate-dependent slip of Newtonian liquid at smooth surfaces, Physical review letters, 87 (2001).
[52] C. Cottin-Bizonne, B. Cross, A. Steinberger, E. Charlaix, Boundary slip on smooth hydrophobic surfaces: Intrinsic effects and possible artifacts, Physical review letters, 94 (2005).
[53] Y.X. Zhu, S. Granick, Limits of the hydrodynamic no-slip boundary condition, Physical review letters, 88 (2002).
[54] A. Keerthi, A.K. Geim, A. Janardanan, A.P. Rooney, A. Esfandiar, S. Hu, S.A. Dar, I.V. Grigorieva, S.J. Haigh, F.C. Wang, B. Radha, Ballistic molecular transport through two-dimensional channels, Nature, 558 (2018) 420-+.
[55] D.Y. Li, Y.L. Wang, Y.L. Pan, X.Z. Zhao, Measurements of slip length for flows over graphite surface with gas domains, Appl. Phys. Lett., 109 (2016) 4.
[56] Z.T. Li, Y.J. Wang, A. Kozbial, G. Shenoy, F. Zhou, R. McGinley, P. Ireland, B. Morganstein, A. Kunkel, S.P. Surwade, L. Li, H.T. Liu, Effect of airborne contaminants on the wettability of supported graphene and graphite, Nature materials, 12 (2013) 925-931.
[57] R. Raj, S.C. Maroo, E.N. Wang, Wettability of Graphene, Nano Letters, 13 (2013) 1509-1515.
[58] D. Ortiz-Young, H.C. Chiu, S. Kim, K. Voitchovsky, E. D. Ortiz-Young, The interplay between apparent viscosity and wettability in nanoconfined water, Nature communications, 4 (2013).
[59] K.L. Wu, Z.X. Chen, J. Li, X.F. Li, J.Z. Xu, X.H. Dong, Wettability effect on nanoconfined water flow, Proceedings of the National Academy of Sciences of the United States of America, 114 (2017) 3358-3363.
[60] H.B. Zeng, K.L. Wu, X. Cui, Z.X. Chen, Wettability effect on nanoconfined water flow: Insights and perspectives, Nano Today, 16 (2017) 7-8.
[61] D. Feng, X. Li, X. Wang, J. Li, X. Zhang, Capillary filling under nanoconfinement: The relationship between effective viscosity and water-wall interactions, Int. J. Heat Mass Transf., 118 (2018) 900-910.
[62] H. Wang, Y.L. Su, W.D. Wang, G.L. Sheng, H. Li, A. Zafar, Enhanced water flow and apparent viscosity model considering wettability and shape effects, Fuel, 253 (2019) 1351-1360.
[63] E. Bonaccurso, H.J. Butt, V.S.J. Craig, Surface roughness and hydrodynamic boundary slip of a newtonian fluid in a completely wetting system, Physical review letters, 90 (2003) 144501.
[64] Y. Diao, G. Greenwood, M.C. Wang, S. Nam, R.M. Espinosa-Marzal, Slippery and Sticky Graphene in Water, ACS nano, DOI 10.1021/acsnano.8b08666(2019).
[65] Y.L. Pan, B. Bhushan, X.Z. Zhao, The study of surface wetting, nanobubbles and boundary slip with an applied voltage: A review, Beilstein J. Nanotechnol., 5 (2014).
[66] J. Cohen, Statistical Power Analysis for the Behavioral Sciences (2 nd), DOI (1988).
[67] J.E. Freund, B.M. Perles, Modern elementary statistics, DOI (2013).
[68] N. Kavokine, M.L. Bocquet, L. Bocquet, Fluctuation-induced quantum friction in nanoscale water flows, Nature, 602 (2022) 84-+.